Redox Biology 78 (2024) 103423

Contents lists available at ScienceDirect

Redox Biology

journal homepage: www.elsevier.com/locate/redox

Activation of receptor-independent fluid-phase pinocytosis promotes foamy monocyte formation in atherosclerotic mice

WonMo Ahn [a,3], Faith N. Burnett [a,3], Kamila Wojnar-Lason [a], Jaser Doja [a], Amritha Sreekumar [a], Pushpankur Ghoshal [a,1], Bhupesh Singla [a,2], Graydon Gonsalvez [c], Ryan A. Harris [d], Xiaoling Wang [d], Joseph M. Miano [a], Gábor Csányi [a,b,*]

[a] Vascular Biology Center, Augusta University, Medical College of Georgia, Augusta, GA, 30912, USA
[b] Department of Pharmacology and Toxicology, Augusta University, Medical College of Georgia, Augusta, GA, 30912, USA
[c] Department of Cellular Biology & Anatomy, Augusta University, Medical College of Georgia, Augusta, GA, 30912, USA
[d] Georgia Prevention Institute, Augusta University, Medical College of Georgia, Augusta, GA, 30912, USA

ARTICLE INFO

Keywords:
Monocyte
Macropinocytosis
nLDL
Ox-LDL
Hypercholesterolemia
Atherosclerosis

ABSTRACT

Atherosclerotic cardiovascular disease (ASCVD) is the leading cause of death worldwide. Clinical and experimental data demonstrated that circulating monocytes internalize plasma lipoproteins and become lipid-laden foamy cells in hypercholesterolemic subjects. This study was designed to identify the endocytic mechanisms responsible for foamy monocyte formation, perform functional and transcriptomic analysis of foamy and non-foamy monocytes relevant to ASCVD, and characterize specific monocyte subsets isolated from the circulation of normocholesterolemic controls and hypercholesterolemic patients. We hypothesized that activation of fluid-phase macropinocytosis contributes to foamy monocyte formation *in vitro* and in hypercholesterolemic mice *in vivo*. High resolution scanning electron microscopy (SEM) and quantification of FITC/TRITC-dextran internalization demonstrated macropinocytosis stimulation in human (THP-1) and *wild type* murine monocytes. Stimulation of macropinocytosis induced foamy monocyte formation in the presence of unmodified, native LDL (nLDL) and oxidized LDL (ox-LDL) *in vitro*. Genetic blockade of macropinocytosis (***LysMCre***+ $Nhe1^{f/f}$) inhibited foamy monocyte formation in hypercholesterolemic mice *in vivo* and attenuated monocyte adhesion to atherosclerotic aortas *ex vivo*. Mechanistic studies identified NADPH oxidase 2 (Nox2)-derived superoxide anion ($O_2^{\cdot-}$) as an important downstream signaling molecule stimulating macropinocytosis in monocytes. qRT-PCR identified CD36 as a major scavenger receptor that increases in response to lipid loading in monocytes and deletion of CD36 ($Cd36^{-/-}$) inhibited foamy monocyte formation in hypercholesterolemic mice. Bulk RNA-sequencing characterized transcriptional differences between non-foamy and foamy monocytes versus macrophages. Finally, flow cytometry analysis of CD14 and CD16 expression demonstrated a significant increase in intermediate monocytes in hypercholesterolemic patients compared to normocholesterolemic controls. These results provide novel insights into the mechanisms of foamy monocyte formation and potentially identify new therapeutic targets for the treatment of atherosclerosis.

1. Introduction

Atherosclerosis, the primary driver of ischemic heart disease and stroke, accounts for 1 out of every 3 deaths in the United States [1]. Thus, attenuation of atherosclerotic lesion formation and prevention of its cardiovascular complications is an urgent medical need and one of the most serious challenges in cardiovascular medicine. Transmigration of monocytes across the endothelial layer and their differentiation into macrophages play an important role in the initiation and progression of atherosclerosis [2]. The general consensus is that these monocyte-derived macrophages internalize sub-endothelially trapped

* Corresponding author. CB3213A, 1459 Laney Walker Blvd., Augusta University, Medical College of Georgia, Augusta, GA, 30912, USA.
E-mail address: gcsanyi@augusta.edu (G. Csányi).
[1] Present address: Maryland Cannabis Administration, Linthicum, MD, 21090, USA.
[2] Present address: Department of Pharmaceutical Sciences, College of Pharmacy, University of Tennessee Health Science Center, Memphis, TN, 38163, USA.
[3] Authors contributed to the manuscript equally.

https://doi.org/10.1016/j.redox.2024.103423
Received 27 September 2024; Received in revised form 25 October 2024; Accepted 5 November 2024
Available online 6 November 2024

Abbreviations:

AAV8-PCSK9 proprotein convertase subtilisin/kexin type 9 adeno-associated virus serotype 8
Apoe$^{-/-}$: global apolipoprotein E homozygous knockout mice
AUC area under curve
BMI body mass index
CAT catalase
CCL: chemokine ligand
CCR chemokine receptor
CD cluster of differentiation 68
cofilin actin filament regulating protein
CXCL: C-X-C motif chemokine ligand
CXCR C-X-C motif chemokine receptor
CX3CR C-X3-C motif chemokine receptor
Cd36$^{-/-}$: scavenger receptor class B member homozygous knockout mice
DPI diphenyleneiodonium chloride
EGF epidermal growth factor
EIPA 5-(N-Ethyl-N-isopropyl) amiloride
FACS fluorescence-activated cell sorting
FBS fetal bovine serum
FH familial hypercholesterolemia
FITC fluorescein isothiocyanate
FMO fluorescence minus one
GSK2795039 NOX2 inhibitor
HAEC human aortic endothelial cell
HbA1c glycated hemoglobin A1C
ICAM intercellular adhesion molecule
ITGA integrin subfamily A
ITGB integrin subfamily B
LDL: low density lipoprotein
LDLR low density lipoprotein receptor
LOX-1 oxidized low density lipoprotein receptor 1
LysMCre^{+} myeloid cell specific Cre recombinase
M-CSF macrophage colony stimulating factor
MERTK myeloid-epithelial-reproductive tyrosine kinase
NCF neutrophil cytosolic factor
Nhe1$^{f/f}$ floxed sodium hydrogen exchanger 1 mice
Nhe1$^{\Delta M}$ myeloid cell sodium hydrogen exchanger 1 deleted mice
nLDL: native LDL
NOX2 NADPH oxidase 2
$O_2^{\cdot-}$ superoxide anion
ox-LDL: oxidized LDL
PBMC peripheral blood mononuclear cell
PBS phosphate-buffered saline
PCAM platelet endothelial cell adhesion molecule
PDGF platelet-derived growth factor
PFA paraformaldehyde
PKC protein kinase C
PMA phorbol 12-myristate 13-acetate
qRT-PCR quantitative reverse transcriptase polymerase chain reaction
RBC red blood cell
RLU relative light units
SEL: selectin
SEM scanning electron microscopy
SOD superoxide dismutase
SR scavenger receptor
SR-A1 class A1 scavenger receptor
SSC side scatter
TNF-α: tumor necrosis factor alpha
TRITC tetramethylrhodamine
TRL: triglyceride

modified LDL and become lipid-laden foam cells in the arterial wall. Foam cells play a central role in the development of non-resolving arterial inflammation and pathogenesis of atherosclerosis [3]. The accumulation of arterial foam cells promote plaque growth and may contribute to destabilization of atherosclerotic lesions, leading to rupture, thrombosis and reduced oxygen supply to cardiac and brain tissue [4]. Modern medical therapies to combat atherosclerosis have primarily focused on lowering plasma LDL levels in order to decrease the supply of cholesterol-rich lipoproteins that infiltrate the arterial wall and internalize into macrophages [5]. Despite these therapeutic advances, atherosclerotic cardiovascular disease remains the leading cause of death in the United States and globally, underscoring the need for novel and alternative therapeutic strategies to combat this disease [6].

Previous studies in both mice and humans with hyperlipidemia have shown that monocytes are also capable of internalizing plasma lipoproteins from the circulation [7,8]. Foamy monocytes represent ~75 % of total circulating monocytes in patients with familial hypercholesterolemia (FH) and pharmacological depletion of foamy monocytes inhibits atherosclerosis development in hypercholesterolemic mice [7,8]. Although these studies suggest that monocyte uptake of plasma LDL is a therapeutic target in atherosclerosis, the precise mechanism responsible for foamy monocyte formation remains unknown. Monocytes have shown to internalize oxidatively modified LDL (ox-LDL) through scavenger receptors (SR) *in vitro*, specifically scavenger receptor CD36 [7,9]. However, *Cd36*$^{-/-}$ mice are only partially protected from atherosclerosis [10-12] and there is only a partial (~30 %) decrease of circulating foamy monocytes in *Cd36*$^{-/-}$ mice [7]. In addition, ox-LDL represents a relatively small proportion of plasma LDL [13] and scavenger receptors exhibit little affinity for unmodified, native LDL (nLDL) [14,15]. These results suggest that other, yet unidentified, pathways also contribute to monocyte lipid internalization and foam cell formation in hypercholesterolemic patients and experimental animals. Importantly, therapeutic manipulation of circulating foam cells may be more feasible than targeting foam cells accumulating in the arterial wall or promoting arterial reverse cholesterol transport from tissue resident foam cells.

Macropinocytosis is a highly conserved, actin-dependent endocytic process by which extracellular fluid and pericellular solutes are internalized into cells [16]. Macropinocytosis begins with plasma membrane ruffling, followed by formation of macropinocytotic cups, cup closure, and internalization of extracellular fluid and associated solutes via large, heterogeneous vesicles known as macropinosomes [17]. Previous studies have demonstrated that stimulation of macropinocytosis in macrophages increases nLDL internalization and foam cell formation *in vitro* [18,19]. Furthermore, pharmacological inhibition of macropinocytosis and genetic blockade of macropinocytosis specifically in myeloid cells attenuate atherosclerosis development in hypercholesterolemic mice [19]. Macropinocytosis is a unique form of endocytosis as extracellular solutes (*e.g.* LDL) do not require a physical or specific interaction with the plasma membrane (i.e.: receptor binding) in order to be internalized. Consequently, LDL internalization by macropinocytosis does not show receptor saturation and increases with extracellular concentration [18].

To our knowledge, no previous studies have investigated the role of macropinocytosis in foamy monocyte formation *in vitro* or in hypercholesterolemic mice *in vivo*. This study was designed to investigate the role of macropinocytosis in foamy monocyte formation, performed functional and transcriptomic analysis of foamy and non-foamy monocytes relevant to the pathogenesis of atherosclerosis, determined the role of phagocyte NADPH oxidase (NOX2) in macropinocytosis stimulation in monocytes, and characterized subset frequencies of isolated human

monocytes (classical, intermediate and nonclassical) from normocholesterolemic controls and hypercholesterolemic patients.

2. Materials and methods

2.1. Reagents

Phorbol 12-myristate 13-acetate (PMA), 5-(N-Ethyl-N-isopropyl) amiloride (EIPA), diphenyleneiodonium chloride (DPI), superoxide dismutase (SOD), catalase (CAT), sodium orthovanadate, and Triton X-100 were purchased from Sigma-Aldrich (St. Louis, MO, USA). FITC-dextran (70 kDa), Hoechst 33342, Alexa fluor 488 phalloidin, Nile Red, Amplex Red Cholesterol Assay Kit, RPMI-1640 medium, human recombinant TNFα, RIPA lysis buffer, Pierce BCA protein assay kit, Pierce protease and phosphatase inhibitor mini tablets, and anti-human monoclonal antibodies CD14-BV421, and CD16-FITC were purchased from ThermoFisher (Waltham, MA, USA). Anti-human monoclonal antibody CD115-APC was purchased from BioLegend (San Diego, CA, USA). Anti-Perilipin-2-AF488 monoclonal and AF488-IgG1 isotype control antibodies were purchased from Bio-Techne (Minneapolis, MN, USA). Human native LDL (nLDL) and human medium oxidized LDL (ox-LDL) were purchased from Kalen Biomedical (Montgomery Village, MD, USA). Primers for genotyping and scavenger receptor primers for quantitative real-time PCR were purchased from Integrated DNA Technologies (Coralville, IA, USA). AAV8-PCSK9 was obtained from Charles River Laboratories International (Charleston, SC, USA). Small molecule NADPH oxidase 2 (NOX2) inhibitor GSK 2795039 was purchased from Tocris Bioscience (Bristol, UK). L-012 was purchased from Fujifilm (Tokyo, Japan). Western blot primary antibodies for NOX2 (EPR6991), MERTK (Y-323), and GAPDH were purchased from Abcam (Cambridge, UK). Western blot primary antibodies for cofilin and P-cofilin (SER-3) were purchased from Cell Signaling Technology (Danvers, MA, USA). Human and mouse CD11b microbead kit, Mouse CD115 microbead kit, Mouse Bone Marrow Isolation kit, Human pan monocyte isolation kit, MS columns, and LS columns were purchased from Miltenyi Biotec (North Rhine-Westphalia, Germany). THP-1 monocytes were purchased from ATCC (Manassas, VA, USA). Human aortic endothelial cells (HAEC), EBM-2 MV medium, and the supplemental EGM-2 MV kit were purchased from Lonza (Gampel-Bratsch, Switzerland). Lympholyte Cell Separation Media was purchased from Cedar Lane Labs (Ontario, Canada). BD vacutainer CPT tubes were purchased from BD Bioscience (Franklin Lakes, NJ, USA). TaqMan Reverse Transcriptase kit and SYBR Green Super mix were purchased from Applied Biosystems (Grand Island, NY, USA). Laemmli sample buffer was purchased from BIORAD Laboratories Inc. (Hercules, CA, USA). Protein-Free Blocking Buffer and IRDye-conjugated secondary antibodies were purchased from (Li-Cor Biosciences, Lincoln, NE, USA).

2.2. Cell culture

All cells were cultured in humidified incubators at 37 °C and 5 % CO_2. Human THP-1 monocytes (ATCC, Manassas, Virginia, USA) were grown in RPMI-1640 medium supplemented with 10 % FBS, 100 IU/ml of penicillin G and 100 μg/ml streptomycin. Human aortic endothelial cells (HAECs) (Lonza, Houston, TX, USA) were cultured in EBM-2 MV medium supplemented with the EGM-2 MV kit (Lonza). Primary murine bone marrow and splenic monocytes were cultured in RPMI-1640 medium supplemented with 10 % FBS, 100 IU/ml of penicillin G and 100 μg/ml streptomycin. Monocytes were incubated in starvation media (1 % FBS) for 24 h prior to experiments.

2.3. Animals

All mice were housed in accordance with the National Institutes of Health (NIH) guidelines in our AALAC-accredited experimental animal facility in a controlled environment. All mouse studies were approved by the Institutional Animal Care and Use Committee at Augusta University (#2014-0704). C57BL/6J wild-type (stock #000664), *Cd36*$^{-/-}$ (stock #019006), *Apoe*$^{-/-}$ (stock #002052), and *LysMCre* (stock #019096) were purchased from The Jackson Laboratory (Bar Harbor, ME, USA). *Nhe1*$^{f/f}$ mice were provided by Dr. Dandan Sun (University of Pittsburgh, Department of Neurology, Pittsburgh, USA). *LysMCre* + *Nhe1*$^{f/f}$ (*Nhe1*$^{\Delta M}$) mice were generated by crossing *Nhe1*$^{f/f}$ and *LysMCre* + mice. Littermate *LysMCre*$^{-}$ *Nhe1*$^{f/f}$ (*Nhe1*$^{f/f}$) mice were used as controls. All mice were genotyped via PCR amplification of tail DNA. To induce hypercholesterolemia, AAV8-PCSK9 (Charles River Laboratories International, Charleston, SC, USA) (1 x 10^{11} VG) was injected retro-orbitally into *wild type*, *Cd36*$^{-/-}$, *Nhe1*$^{f/f}$ and *Nhe1*$^{\Delta M}$ mice. After injections, mice were placed on a Western diet (Envigo, Indianapolis, IN, USA) for 16-20 weeks. All other mice were fed a standard chow diet. Prior to primary cell isolation, mice were anesthetized (isoflurane inhalation, 3 %) and exsanguinated. Every effort was made to minimize animal suffering and reduce the number of animals used.

2.4. Primary murine monocyte isolation

2.4.1. Bone-marrow monocyte isolation

The femur and tibia of 4-month-old male *C57*BL*/6J wild type*, *Cd36*$^{-/-}$, *Nhe1*$^{f/f}$, and *Nhe1*$^{\Delta M}$ mice were cleaned of muscle and connective tissue. Both ends of each bone were cut and the bone marrow was flushed out using a 25-gauge needle syringe containing 1x Phosphate Buffered Saline (PBS) containing (1 % FBS, 100 IU/ml of penicillin G and 100 μg/ml streptomycin). Bone marrow cell count was determined using the Countess II Automated Cell Counter (Life Technologies, Carlsbad, CA, USA). Non-monocytic cells were then magnetically labeled using the Monocyte Bone Marrow Isolation Kit (Miltenyi Biotec, North Rhine-Westphalia, Germany) and depleted using the LS MACS Column (Miltenyi Biotec) and the QuadroMACS Separator (Miltenyi Biotec). Isolated monocytes were cultured in RPMI-1640 medium (10 % FBS, 100 IU/ml of penicillin G and 100 μg/ml streptomycin).

2.4.2. Splenic monocyte isolation

The spleens of 3-month-old male *C57*BL*/6J wild type* and male 7-month-old *Apoe*$^{-/-}$ (Western diet 4 months) mice were dissected and mechanically digested using the back end of a 1 mL syringe. Splenic cells were passed through a Falcon Cell Strainer (100 μm) (Fisher Scientific, Hampton, NH, USA) and centrifuged at 300 *g* for 10 min. Red blood cells (RBC) were lysed by resuspending the pellet in 1x RBC Lysis Buffer (ThermoFisher, Waltham, MA, USA) and incubating for 5 min with gentle agitation. RBC-free cells were sedimented by centrifugation at 300*g* for 10 min and counted using the Countess II Automated Cell Counter (Life Technologies). Monocytes were then magnetically labeled with the CD115 MicroBead Kit (Miltenyi Biotec) and purified using the MS MACS Column (Miltenyi Biotec) and the OctoMACS Separator (Miltenyi Biotec). Isolated monocytes were cultured in RPMI-1640 medium (10 % FBS, 100 IU/ml of penicillin G and 100 μg/ml streptomycin).

2.4.3. Blood monocyte isolation

Blood from male 7-month-old hypercholesterolemic (AAV8-PCSK9, Western diet 4 month) *wild type*, *Cd36*$^{-/-}$, *Nhe1*$^{f/f}$, and *Nhe1*$^{\Delta M}$ mice was collected from the left ventricle using a heparinized syringe fitted with a 21-gauge needle. Blood was then diluted in a 1:1 ratio with 1x PBS and carefully layered onto a density gradient medium (1.085 g/cm^3) (Lympholyte Cell Separation Media, Cedar Lane Labs, Ontario, Canada). After centrifugation (400 *g*, 40 min, deceleration 0), Peripheral blood mononuclear cells (PBMCs) were isolated and washed twice with 1x PBS (1 % FBS). Cells were counted using the Countess II Automated Cell Counter (Life Technologies) and monocytes were magnetically labeled with the CD11b MicroBead Kit (Miltenyi Biotec). Monocytes were then purified using MS MACS Columns (Miltenyi Biotec) and the OctoMACS Separator (Miltenyi Biotec). Isolated monocytes were cultured in RPMI-1640

medium (10 % FBS, 100 IU/ml of penicillin G and 100 μg/ml streptomycin).

2.5. Isolation of primary human monocytes

All human studies were approved by the Institutional Review Board at Augusta University (#1323570, #1638053). A single stick blood draw was performed to obtain whole blood from both male and female individuals between the ages of 18 and 50 years old. Blood was obtained following an overnight fast. A lipid panel was obtained using standardized clinical core laboratory techniques (Laboratory Corporation of America Holdings, Birmingham, AL, USA). The lipid profiles for normal and hypercholesterolemic individuals are shown in Suppl. Table 3. Approximately, 10 mL of whole blood from each participant was drawn into BD Vacutainer CPT tubes (BD Bioscience, Franklin Lakes, NJ, USA) and diluted in a 1:1 ratio with 1x PBS. The diluted blood was layered onto a density gradient medium (1.085 g/cm^3) (Lympholyte Cell Separation Media, Cedar Lane Labs) and centrifuged (400 *g*, 40 min, deceleration 0). PBMCs were isolated, washed twice with 1x PBS (1 % FBS) and counted using the Countess II Automated Cell Counter (Life Technologies). Non-monocytic cells were magnetically labeled with the Pan Monocyte Isolation Kit (Miltenyi Biotec) and depleted using the LS MACS Column (Miltenyi Biotec) and the QuadroMACS Separator (Miltenyi Biotec). Isolated monocytes were fixed with 4 % paraformaldehyde (PFA) for 30 min at 4 °C and resuspended in 1x PBS.

2.6. Scanning electron microscopy

2.6.1. Quantification of monocyte macropinocytosis

Human THP-1 monocytes (ATCC) were seeded onto human aortic endothelial cells (HAEC, ATCC). Endothelial cells were preincubated with human recombinant TNFα (10 ng/ml) for 4 h to promote their expression of adhesion molecules. Once adhered, monocytes were treated with vehicle or phorbol 12-myristate 13-acetate (PMA) (1 μM, 20 min) ± 5-(N-Ethyl-N-isopropyl) amiloride (EIPA) (25 μM, 30 min pre-incubation). Monocytes were fixed (4 % PFA, 2 % glutaraldehyde in 0.1 M sodium cacodylate solution) at 4 °C for 16 h. Cells were dehydrated with graded concentrations of ethanol (25%–100 %) and underwent critical point drying (Tousimis Samdri-790, Rockville, MD, USA). Cells were then sputter coated with 3.5 nm of gold palladium (Anatek USA-Hummer, Sparks, NV, USA) and imaged at 20 KV using a JEOL JSM-IT500HR InTouchScope Scanning Electron Microscope (Tokyo, Japan). Monocyte membrane ruffles were normalized to the cell number in the microscopic field of view and quantified.

2.6.2. Adhesion of primary monocytes to atherosclerotic aortic lesions

Murine splenic monocytes were isolated from hypercholesterolemic (AAV8-PCSK9, Western diet 4 months) *Nhe1*$^{f/f}$ and *Nhe1*$^{\Delta M}$ mice. Monocytes were incubated with atherosclerotic aortic arch segments isolated from hypercholesterolemic *Nhe1*$^{f/f}$ mice (AAV8-PCSK9, Western diet 4 months) in a tissue culture incubator at 37 °C and 5 % CO_2 for 3 h. Aortic tissues were fixed (4 % PFA, 2 % glutaraldehyde in 0.1 M sodium cacodylate solution) at 4 °C for 16 h and processed for scanning electron microscopy as described above. Twenty random images from the inner curvature of aortic arch were captured at x3,300 magnification and the number of monocytes per microscopic field of view was quantified.

2.7. Flow cytometry

Flow cytometry experiments were performed using the Acea 4-Laser Novocyte Quanteon flow cytometer (Agilent, Santa Clara, CA, USA). A minimum of 10,000 events were collected for all experiments.

2.7.1. Quantification of macropinocytosis-mediated solute uptake in vitro

Murine or human monocytes were treated with vehicle, PMA (1 μM) ± EIPA (25 μM, 30 min pre-incubation) in the presence of FITC-dextran (100 μg/mL, 3 h, 70 kDa, fluid-phase marker) or TRITC-dextran (100 μg/mL, 3 h, 70 kDa, fluid-phase marker). In separate experiments, monocytes were treated with vehicle or PMA (1 μM, 3 h), in the absence or presence of superoxide dismutase (SOD) (150 U/mL, 30 min pre-incubation), catalase (CAT) (800 U/mL, 30 min pre-incubation), diphenyleneiodonium chloride (DPI) (5 μM, 30 min pre-incubation) or GSK2795039 (20 μM, 30 min pre-incubation), and FITC-dextran uptake was quantified. Macropinocytic uptake of FITC-dextran was quantified by measuring FITC fluorescence intensity (Ex: 488 nm, Em 530/30 nm). Macropinocytic uptake of TRITC-dextran was quantified by measuring TRITC fluorescence intensity (Ex: 561 nm, Em 586/20 nm).

2.7.2. Foamy monocyte formation in vitro

Human THP-1 monocytes were treated with PMA (1 μM, 24 h) ± EIPA (25 μM, 30 min pre-incubation) in the presence of native LDL (nLDL) (Kalen Biomedical) (50 μg/mL, 24 h) or oxidized LDL (ox-LDL) (Kalen Biomedical) (50 μg/mL, 24 h). Monocytes were collected and stained with Nile Red (50 ng/mL, 10 min) (ThermoFisher, Waltham, MA, USA). In separate experiments, murine bone marrow monocytes from *wild type* and *Cd36*$^{-/-}$ mice were treated with PMA (1 μM, 24 h) in the presence of nLDL (50 μg/mL, 24hr) or ox-LDL (50 μg/mL, 24 h) and stained with Nile Red (50 ng/mL, 10 min). Next, blood monocytes from hypercholesterolemic (AAV8-PCSK9) *wild type*, *Cd36*$^{-/-}$, *Nhe1*$^{f/f}$, and *Nhe1*$^{\Delta M}$ mice were isolated and stained with Nile Red (50 ng/mL, 10 min). A similar experiment was performed using blood and splenic monocytes from hypercholesterolemic *Apoe*$^{-/-}$ mice. In all experiments, Nile Red fluorescence intensity was measured (Ex: 488 nm, Ex: 586/20 nm).

Finally, THP-1 monocytes were treated with PMA (1 μM, 24 h) in the presence of ox-LDL (50 μg/mL, 24hr). Cells were permeabilized with Triton X-100 (0.1 %, 5 min) and stained with a monoclonal anti-Perilipin-2-AF488 antibody or AF488-IgG1 isotype control (Bio-Techne, Minneapolis, MN, USA) (5.9 μg/100 μL, 1hr). AF488 fluorescence intensity was measured (Ex: 488 nm, Ex: 530/30 nm). Mean side scatter (SSC) was quantified for perilipin-2 positive and perilipin-2 negative monocytes.

2.7.3. Characterization of human monocyte subsets

Hypercholesterolemic patients were defined as patients with total cholesterol >200 mg/dL. Normocholesterolemic patients were defined as patients with total cholesterol <180 mg/dL). Primary human blood monocytes from normocholesterolemic and hypercholesterolemic patients were isolated, fixed with 4 % PFA and incubated with anti-human monoclonal CD115-APC (BioLegend, San Diego, CA, USA), CD16-FITC, and CD14-BV421 (ThermoFisher) (1 μg/100 μL, 1 h) antibodies. Fluorescence minus one (FMO) controls were used to determine the appropriate gating strategy for each fluorescence signal. CD14-BV421 (Ex: 405 nm, Em: 445/45 nm) and CD16-FITC (Ex: 488 nm, Em: 530/30 nm) fluorescence intensities were determined in CD115-APC (Ex: 640 nm, Em: 660/20)-gated monocytes to quantify the percentage of classical, intermediate, and nonclassical monocyte subsets. CD14 and CD16 double negative cells were excluded from the analysis. Mean side scatter (SSC) for each subset was quantified to identify foamy monocytes.

2.8. Confocal imaging

Imaging was performed using a Zeiss 780 inverted confocal microscope. Human THP-1 monocytes (ATCC) were stained with Hoechst 33342 (ThermoFisher) and seeded onto HAEC pretreated with human recombinant TNF-α (10 ng/ml, 4 h). Once adhered, monocytes were treated with vehicle or PMA (1 μM, 20 min) ± EIPA (25 μM, 30 min pre-incubation) in the presence of nLDL (50 μg/mL, 24 h) or ox-LDL (50 μg/mL, 24 h). Cells were fixed with 4 % PFA (30 min) and stained with AlexaFluor 488 Phalloidin (ThermoFisher) (6.6 μM) and Nile Red (50

ng/mL, 10 min). Cells were imaged at 63x. Nile Red positive lipid droplets were normalized to the cell number in the microscopic field of view and quantified using the ImageJ software (NIH).

2.9. Plasma cholesterol measurement

Total concentrations of plasma cholesterol were measured using the Amplex Red Cholesterol Assay Kit (ThermoFisher) according to the manufacturer's protocol.

2.10. qRT-PCR

Total RNA was isolated from bone marrow-derived monocytes using an RNA extraction kit (IBI Scientific, Dubuque, Iowa, USA) according to the manufacturer's protocol. The NanoDrop Microvolume Spectrophotometer (ThermoFisher) was used to determine RNA concentration and quality based on each sample's optical density at 260 nm and 280 nm. The TaqManReverse Transcriptase kit (Applied Biosystems, Grand Island, NY, USA) was used to generate complementary DNA from RNA. Real-time PCR was performed using the SYBR Green Super mix (Applied Biosystems). All amplifications were performed in triplicates and normalized to GAPDH. The $\Delta\Delta C_t$ method was used to quantify expression. The primer sequences used for real time PCR are shown in Suppl. Table 2.

2.11. Bulk RNA sequencing

Murine splenic monocytes were isolated from 3-month-old male *wild type* mice as previously described. Monocytes were differentiated into macrophages using PMA (200 ng/mL, 5 days). Monocytes and differentiated macrophages were treated with vehicle or ox-LDL (50 μg/mL, 24 h). Total RNA was extracted using an RNA extraction kit (IBI Scientific, Dubuque, Iowa, USA) according to the manufacturer's protocol. Samples were frozen and shipped to the Genome Technology Access Center at the McDonnell Genome Institute at Washington University School of Medicine for processing. Total RNA integrity was determined using Agilent Bioanalyzer or 4200 Tapestation (Santa Clara, CA, USA). Library preparation was performed with 10 ng of total RNA with a Bioanalyzer RIN score greater than 8.0. ds-cDNA was prepared using the SMARTer Ultra Low RNA kit for Illumina Sequencing (Takara-Clontec, San Jose, CA, USA) per manufacturer's protocol. cDNA was fragmented using a Covaris E220 sonicator (Woburn, MA, USA) using peak incident power 18, duty factor 20 %, cycles per burst 50 for 120 s cDNA was blunt ended, had an A base added to the 3′ ends, and then had Illumina sequencing adapters ligated to the ends. Ligated fragments were then amplified for 12-15 cycles using primers incorporating unique dual index tags. Fragments were sequenced on an Illumina NovaSeq X Plus (San Diego, CA, USA) using paired end reads extending 150 bases. Basecalls and demultiplexing were performed with Illumina's bcl2fastq software with a maximum of one mismatch in the indexing read. RNA-seq reads were then aligned to the Ensembl release 101 primary assembly with STAR version 2.7.9a1. Gene counts were derived from the number of uniquely aligned unambiguous reads by Subread:featureCount version 2.0.32. Isoform expressions of known Ensembl transcripts were quantified with Salmon version 1.5.23. Sequencing performance was assessed for the total number of aligned reads, total number of uniquely aligned reads, and features detected. The ribosomal fraction, known junction saturation, and read distribution over known gene models were quantified with RSeQC version 4.04.

2.12. Western blot

THP-1 monocytes were treated with vehicle or PMA (1 μM) for different durations (5 min–60 min or 1 h–1 week). In a separate experiments, THP-1 monocytes were treated with vehicle or ox-LDL (50 μg/mL, 24 h). Cell lysates were prepared using 1x RIPA Lysis Buffer (ThermoFisher) supplemented with Pierce Protease and Phosphatase Inhibitor Mini Tablets (ThermoFisher). Protein concentration was quantified using the Pierce BCA Protein Assay Kit (ThermoFisher). Proteins (25 μg) were heated in Laemmli sample buffer (BioRad Laboratories Inc., Hercules, CA, USA) for 5 min at 95 °C, separated on 10 % SDS-PAGE gels and transferred onto nitrocellulose membranes (Li-Cor Biosciences, Lincoln, NE, USA) overnight at 25 V in 4 °C. The membranes were blocked with Protein-Free Blocking Buffer (Li-Cor Biosciences) for 1 h and probed with primary antibodies for cofilin, p-cofilin (SER-3) (Cell Signaling Technology, Danvers, MA, USA), NOX2 (EPR6991), MERTK (Y-323), or GAPDH (Abcam, Cambridge, UK) overnight at 4 °C. IRDye-conjugated secondary antibodies (Li-Cor Biosciences) were used to detect the membrane-bound primary antibodies. Membranes were imaged using the Odyssey CLx Infrared Imaging System (Li-Cor Biosciences).

2.13. Quantification of superoxide anion production using L-012 chemiluminescence

The L-012 chemiluminescent probe (Fujifilm, Tokyo, Japan) was used to determine superoxide anion production in *wild type* splenic and THP-1 monocytes. Fifty thousand cells per well were plated in white-with-transparent bottom 96-well plates (Corning Inc., Corning, NY, USA) in 1x PBS containing 400 μM L-012 and 1 mM Sodium Orthovanadate (Sigma-Aldrich, St. Louis, MO, USA). Cells were pretreated with antioxidant enzymes SOD (Sigma-Aldrich) (150 U/mL, 15 min) or CAT (Sigma-Aldrich) (800 U/mL, 15 min), or NOX2 inhibitors diphenyleneiodonium chloride (DPI) (Sigma-Aldrich) (5 μM, 15 min) or GSK2795039 (Tocris Bioscience) (20 μM, 30 min). Superoxide anion production was stimulated with PMA (1 μM, 3 h). Luminescence (RLU) was measured at 37 °C every 2 min for 3 h and data analyzed using the MARS data analysis software (BMG LABTECH, Ortenberg, Germany). Superoxide anion production was quantified by calculating the area under the curve (AUC).

2.14. Statistical analysis

Statistics and differential gene analysis was performed with DESeq2. Statistical significance was defined with a p-adjusted value < 0.05. All other data were analyzed using GraphPad Prism 10.1.2 (GraphPad Software Inc., Boston, MA, USA). and presented as means ± SD. T-tests or one/two-way analysis of variance (ANOVA) with Tukey's post hoc test was used to analyze differences between groups. Statistical significance was defined as $p < 0.05$.

3. Results

3.1. Stimulation of monocyte macropinocytosis promotes nLDL internalization and foam cell formation in vitro

Macropinocytosis is a receptor-independent endocytic process that mediates non-specific internalization of extracellular fluid and associated pericellular solutes [16]. To our knowledge, macropinocytic membrane activity and solute macropinocytosis in cultured monocytes *in vitro* or circulating monocytes *in vivo* have not been previously demonstrated. Macropinocytosis can be induced in macrophages upon stimulation with phorbol esters (phorbol 12-myristate 13-acetate [PMA]), inflammatory cytokines (interferon-γ [IFN- γ], tumor necrosis factor α [TNF-α]) and growth factors (macrophage colony-stimulating factor-1 [M-CSF], epidermal growth factor [EGF], platelet derived growth factor [PDGF]) [20-23]. In this study, we first investigated whether the chemical macropinocytosis stimulator PMA promotes membrane ruffle formation in monocytes using Scanning Electron Microscopy (SEM). Macropinocytosis is initiated by extensive, sub-membranous activation of the actin cytoskeleton resulting in plasma membrane ruffling that may circularize and form cups, leading to

macropinosome formation and solute internalization [24,25]. THP-1 monocytes adhered to human aortic endothelial cell (HAEC) monolayer exhibited marked membrane ruffling following stimulation with PMA (1 μM, 20 min) (Fig. 1A). Pretreatment of monocytes with the macropinocytosis blocker 5-(N-ethyl-N-isopropyl) amiloride (EIPA) (25 μM, 30 min) inhibited membrane ruffle formation. Quantification of membrane ruffles demonstrated a ~7-fold increase in membrane ruffling following PMA treatment (0.21 ± 0.16 and 1.54 ± 0.09; $*p < 0.05$, for vehicle and PMA treatment, respectively; Fig. 1B). Mer tyrosine kinase (MERTK) is upregulated upon monocyte to macrophage differentiation, and it enables macrophages to efficiently clear apoptotic cells to maintain tissue homeostasis [26]. Importantly, PMA treatment (1 μM) within 6 h did not induce MERTK protein expression in THP-1 cells (Suppl. Figs. 1A–B).

Next, we investigated whether stimulation of membrane ruffling in monocytes is followed by macropinocytotic internalization of fluorescently labeled extracellular solutes. Monocytes were incubated with the fluid-phase marker FITC-dextran (70,000 MW, 100 μg/mL), treated with vehicle or PMA, and uptake was quantified using fluorescence-activated cell sorting (FACS). As shown in Fig. 1C–D, PMA stimulated FITC-dextran internalization in THP-1 monocytes, while pretreatment with the macropinocytosis inhibitor EIPA blunted this effect. Because FITC-dextran is pH sensitive, TRITC-dextran (70,000 MW, 100 μg/mL) was also used to confirm macropinocytosis stimulation in monocytes (Suppl. Fig. 2).

Although foamy monocytes represent ~75 % of total circulating monocytes in hypercholesterolemic patients, the endocytic mechanism (s) responsible for monocyte lipoprotein uptake remains to be identified [8]. Next, we investigated whether stimulation of monocyte macropinocytosis promotes nLDL internalization and foamy monocyte formation *in vitro*. Non-adherent THP-1 monocytes were incubated with nLDL (50 μg/ml) and treated with vehicle or PMA in the absence or presence of EIPA. Intracellular lipids were stained with the fluorescent lipophilic dye Nile Red and lipid accumulation was analyzed by confocal laser microscopy and flow cytometry. As shown in Fig. 1E–G, macropinocytosis stimulation significantly increased lipid accumulation in monocytes, while pretreatment with EIPA inhibited Nile Red fluorescence and lipid droplet formation. Pharmacological blockade of Na^+/H^+ exchanger 1 (NHE1) by EIPA inhibits macropinocytosis in macrophages and other cell types [19,27]. Next, we generated mice lacking NHE1 selectively in myeloid cells ($Nhe1^{\Delta M}$) to inhibit macropinocytosis in monocytes *in vitro and in vivo* (Suppl. Fig. 3). Primers for *Nhe1* and *LysMCre* genotyping are shown in Suppl. Table 1. As shown in Fig. 1H–I, PMA stimulated macropinocytotic uptake of FITC-dextran in bone marrow-derived $Nhe1^{f/f}$ monocytes but not in macropinocytosis-deficient $Nhe1^{\Delta M}$ monocytes. These results suggest that stimulation of macropinocytosis promotes nLDL internalization in monocytes, leading to foam cell formation *in vitro*.

3.2. Scavenger receptors and macropinocytosis contribute to ox-LDL uptake and foamy monocyte formation in vitro

Macrophages internalize oxidatively modified LDL (ox-LDL) through scavenger receptors (SR), specifically SR-A and class SR-B CD36 [28-30]. The role of SR in foamy monocyte formation is not well characterized. qRT-PCR was used to quantify mRNA levels of major SR [class: *Sr-a, Sr-b, Sr-e, Sr-e* and *Sr-others* [31] and low-density lipoprotein receptor (*Ldlr*) in murine *wild type* bone marrow-derived monocytes. Primers used for qRT-PCR are shown in Suppl. Table 2. Lectin-type oxidized LDL receptor 1 (*Lox-1*), class SR-D1 *Cd68*, and *Cd14* receptor showed significantly higher mRNA expression relative to the low expression levels of *Sr-a1* in non-foamy monocytes (Fig. 2A). *Cd36*, *Scara5*, *Sr-b1*, and *Cxcl16* expressions were not different from *Sr-a1* mRNA levels. mRNA levels of *Cd36* and *Cxcl16* were significantly increased in lipid-laden monocytes (ox-LDL, 50 μg/ml, 24 h), however *Lox-1*, *Cd14*, and *Cd68* mRNA levels did not increase in response to lipid loading compared to vehicle-treated controls (Fig. 2B).

Macropinocytosis of nLDL is linearly related to extracellular lipid concentration [17]. On the contrary, modified lipoproteins (*e.g.* ox-LDL) saturate SR at concentrations between 25 and 50 μg/ml [18,32]. The next experiments were designed to investigate the relative contribution of macropinocytosis vs. SR to monocyte LDL internalization *in vitro* using the same experimental conditions (nLDL/ox-LDL: 50 μg/ml, 24 h). THP-1 monocytes were incubated with ox-LDL, treated with vehicle or PMA (1 μM) in the absence or presence of EIPA (25 μM, 30 min), fixed and stained with Nile Red. SR-mediated ox-LDL uptake in monocytes was demonstrated by confocal laser imaging and flow cytometry analysis of Nile Red fluorescence (Fig. 2C–E). Stimulation of macropinocytosis further increased ox-LDL uptake in monocytes, suggesting an additive effect between SR- and macropinocytosis-mediated lipid uptake and foamy monocyte formation (Fig. 2D–E). As shown in Fig. 2F, monocyte uptake of nLDL (50 μg/ml, 24 h) was mediated primarily by macropinocytosis. Contribution of SR vs. macropinocytosis to monocyte uptake of ox-LDL *in vitro* was dependent on both macropinocytosis and SR (Fig. 2F). Furthermore, treatment of monocytes with ox-LDL (50 μg/mL, 24 h) did not induce monocyte to macrophage differentiation as determined by Western blot of MERTK. (Suppl. Figs. 1C–D).

Finally, ox-LDL uptake of monocytes from normocholesterolemic *wild type* and $Cd36^{-/-}$ mice was similar (Fig. 2G–I), consistent with low CD36 expression in non-foamy monocytes (Fig. 2A). Macropinocytosis stimulation increased uptake of nLDL in both *wild type* and $Cd36^{-/-}$ monocytes. Mouse genotyping was performed by PCR using primers specific for the *wild type* and null alleles of *Cd36* (Suppl. Table 1). Taken together, these results suggest that monocytes from normocholesterolemic mice internalize nLDL and ox-LDL via macropinocytosis. In addition, ox-LDL uptake by non-foamy monocytes is independent of CD36.

3.3. Macropinocytosis and SR CD36 mediate lipid uptake and promote foamy monocyte formation in hypercholesterolemic mice in vivo

Next, macropinocytosis-and CD36-dependent lipoprotein uptake was investigated in circulating monocytes in hypercholesterolemic mice *in vivo*. Consistent with previous reports [7], foamy monocyte formation was significantly increased in hypercholesterolemic $Apoe^{-/-}$ mice (4 months Western diet) compared to monocytes isolated from *wild type* mice fed a normal chow diet (Suppl. Figs. 4A–G). Primers for *Apoe* genotyping are shown in Suppl. Table 1. To confirm these results using an alternative model and to investigate the mechanisms of foamy monocyte formation *in vivo*, hypercholesterolemia was induced using AAV8-PCSK9 and Western diet (4 months) in macropinocytosis-deficient $Nhe1^{\Delta M}$ and $Cd36^{-/-}$ mice and their respective controls [33,34]. Circulating $CD11b^+$ monocytes from *wild type* and $Cd36^{-/-}$ mice were isolated, stained with Nile Red, and analyzed via flow cytometry (Fig. 3A). As shown in Fig. 3B, total plasma cholesterol levels were significantly elevated in AAV8-PCSK9-injected *wild type* and $Cd36^{-/-}$ mice compared with normocholesterolemic (no AAV8-PCSK9) controls. Bodyweight was not significantly different between experimental groups (Suppl. Fig. 5B). Loss of CD36 significantly decreased foamy monocyte formation in hypercholesterolemic mice *in vivo* (Fig. 3C–E).

Total plasma cholesterol levels and body weight were similar in AAV8-PCSK9-injected $Nhe1^{f/f}$ control and macropinocytosis-deficient $Nhe1^{\Delta M}$ mice but significantly increased compared to their respective normocholesterolemic controls (Fig. 3F, Suppl. Fig. 5C). Foamy monocyte formation was inhibited in hypercholesterolemic $Nhe1^{\Delta M}$ mice compared to $Nhe1^{f/f}$ controls (Fig. 3G–H). These results suggest that both CD36 and macropinocytosis contribute to foamy monocyte formation in hypercholesterolemic mice *in vivo*.

Adhesion of circulating monocytes to the dysfunctional endothelial layer and their transmigration into the arterial wall play important roles in the development of atherosclerotic lesions [7,35]. Next, the

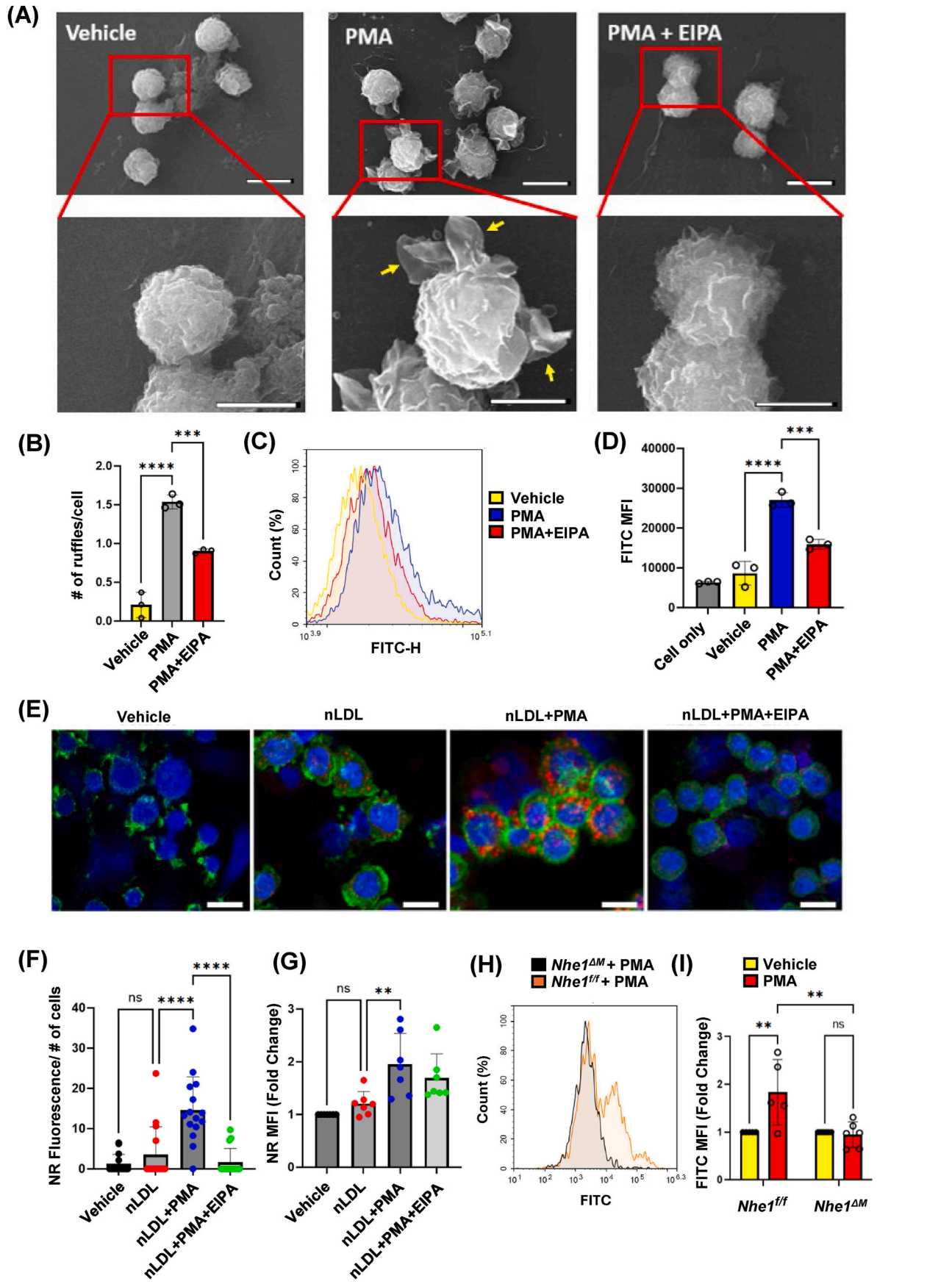

(caption on next page)

Fig. 1. Stimulation of monocyte macropinocytosis promotes nLDL internalization and foam cell formation *in vitro*. THP-1 monocytes were seeded onto confluent HAECs and treated with vehicle or PMA (1 μM, 20 min), ± EIPA (25 μM, 30 min preincubation), and processed for SEM. **(A)** Representative SEM images demonstrating emerging membrane ruffles (yellow arrows) upon PMA stimulation. Scale bar: 10 μm. **(B)** Quantification of the number of membrane ruffles normalized to cell number. ($n = 3$). **(C, D)** THP-1 monocytes were incubated with FITC-dextran (100 μg/ml) and treated with vehicle or PMA (1 μM, 3 h), ± EIPA (25 μM, 30 min preincubation). Internalization of FITC-dextran was quantified via FACS (Ex: 488 nm, Em 530/30 nm). ($n = 3$). **(E)** THP-1 monocytes were treated with vehicle or PMA (1 μM), ± EIPA (25 μM, 30 min pre-incubation) in the presence of nLDL (50 μg/mL, 24hr). Cells were fixed in 4 % PFA and nuclei stained with Hoechst (*blue*); F-actin was labeled with 488 phalloidin (*green*); and lipids were visualized using Nile Red (*red*). Images were taken with a Zeiss 780 inverted confocal microscope. Scale bar: 10 μm. **(F)** Quantification of Nile Red fluorescence normalized to the number of cells in the microscopic field of view. ($n = 3$; individual data points represent technical replicates). **(G)** THP-1 monocytes were treated as described in **(E)**, stained with Nile Red and analyzed via FACS (Ex: 488 nm, Ex: 586/20 nm). ($n = 7$). **(H, I)** Bone marrow monocytes isolated from $Nhe1^{f/f}$ and $Nhe1^{\Delta M}$ mice were incubated with FITC-dextran (100 μg/ml), treated with vehicle or PMA (1 μM, 3 h), and processed for FACS analysis. ($n = 5$–6). Data are presented as means ± SD. ns = not significant; $^{**}p<0.01$; $^{***}p<0.001$; $^{****}p<0.0001$. P values were calculated using one-way (B, D, F, G) or two-way (I) ANOVA with Tukey's test for multiple comparisons. (For interpretation of the references to colour in this figure legend, the reader is referred to the Web version of this article.)

functional significance of macropinocytosis-mediated foamy monocyte formation was investigated *ex vivo* using isolated atherosclerotic arteries and primary monocytes. Monocytes from hypercholesterolemic macropinocytosis-deficient $Nhe1^{\Delta M}$ mice showed significantly decreased adhesion to the inner curvature of atherosclerotic $Nhe1^{f/f}$ aortic arch when compared with monocytes from macropinocytosis-intact $Nhe1^{f/f}$ mice (Fig. 3I–J). Representative images of membrane ruffling on the surface of monocytes adhered to endothelial cells of atherosclerotic aortic arch are shown in Suppl. Fig. 6.

3.4. Differential gene expressions in foamy and non-foamy monocytes and macrophages

Differential gene expression analysis showed significant transcriptomic changes between untreated splenic monocytes and macrophages. Among SR-related genes, *Sr-a1* (*Msr1*), *Cd36*, *Cd68*, and *Cd14* were more highly expressed in macrophages compared to monocytes (Fig. 4A–C). On the other hand, *Lox-1* (*Olr1*), *Cxcl16*, and *Ldlr* were more highly expressed in monocytes (Fig. 4C). Chemokines and chemokine receptors play crucial roles in immune system signaling and monocyte migration [36]. Among chemokines-related genes C-X-C motif chemokine ligand (*Cxcl*) 14 and chemokine ligand (*Ccl*) 4 were downregulated in monocytes compared to macrophages (Suppl. Fig. 7A). Most chemokine receptors (~81 %) that we examined were highly upregulated in monocytes. Only chemokine receptor (*Ccr*) 5, C-X-C chemokine receptor (*Cxcr*) 3, and C-X3-C chemokine receptor (*Cx3cr*) 1 were higher in macrophages (Fig. 4C). Genes related to adhesion molecules showed differential expressions largely based on their respective families. For example, selectins (*Sel*), intercellular adhesion molecules (*Icam*) and platelet endothelial cell adhesion molecules (*Pcam*) were highly upregulated in monocytes compared to macrophages (Fig. 4C). Integrin subfamily (*Itga, Itgb*) gene expression was dependent on the specific subunit analyzed (Fig. 4C). Itga5 was higher in macrophages, but Itga4 was higher in monocytes. Among NOX-related genes, *Nox2* (*Cybb*) expression was higher in macrophages but components of NOX including cytochrome *b*-245 alpha chain (*Cyba*) ($p22^{phox}$), and neutrophil cytosolic factor (*Ncf*)1 ($p47^{phox}$), and 4 ($p40^{phox}$) were found to be higher in monocytes (Fig. 4C). All Bulk RNA sequencing data has been submitted to Gene Expression Omnibus (GEO) (GSE278101).

Gene expression comparison between foamy monocytes and foamy macrophages revealed many similarities with the gene expression comparison between untreated monocytes and macrophages. Overall, ~91 % of all genes analyzed showed no difference between sets (Fig. 4C–F, Suppl. Figs. 7A–B). However, several notable differences were found within genes for chemokines and chemokine receptors. Gene expressions for chemokines *Ccl7*, *Ccl9*, and *Ccl19*, as well as chemokine receptor *Ccr3* were not significantly different between untreated monocytes and macrophages but showed increased expression in foamy monocytes compared to foamy macrophages (Fig. 4C–F, Suppl. Figs. 7A–B).

3.5. Increased NADPH oxidase 2 (NOX2) activity stimulates macropinocytosis in monocytes

To our knowledge, no previous studies have investigated the mechanisms that mediate macropinocytosis in monocytes. Phorbol esters stimulate NOX2 activity and superoxide anion ($O_2^{\cdot-}$) production in phagocytes and signal transduction mediators upstream of NOX2 activation, such as RAC1 and protein kinase C (PKC), promote membrane ruffle formation and macropinocytosis in macrophages [37,38]. The role of NOX2 in monocyte macropinocytosis has not been previously investigated. Western blot experiments demonstrated that monocytes express NOX2 (Fig. 5A). NOX2 protein expression was not different during macropinocytosis stimulation compared to unstimulated controls but was significantly increased 24 h after PMA treatment and comparable to positive control fully differentiated macrophages (Fig. 5B). Superoxide anion production increased in both murine and human THP-1 monocytes during macropinocytosis stimulation (Fig. 5C–D., Suppl. Figs. 8A–B). L-012 chemiluminescence was significantly decreased by incubation with superoxide dismutase (SOD) but not catalase, confirming $O_2^{\cdot-}$ detection in monocytes (Fig. 5C–D., Suppl. Figs. 8A–B). Diphenyleneiodonium (DPI, 10 μM, 30 min), a widely used inhibitor of flavin-containing oxidases and pan-NOX inhibitor, and a recently identified isoform-specific NOX2 blocker [(GSK2795039, 20 μM, 30 min [39] significantly decreased $O_2^{\cdot-}$ production in both human and murine monocytes (Fig. 5C–D., Suppl. Figs. 8A–B). Furthermore, DPI and GSK2795039 inhibited macropinocytosis stimulation in monocytes (Fig. 5E–H). Previous studies have demonstrated that cofilin, an actin-regulating protein, is associated with NOX2-mediated membrane ruffling [37]. These results have shown that PMA dephosphorylates cofilin at Serine-3 (Ser-3) via NOX2, leading to stimulation of macrophage membrane ruffling and macropinocytosis [37]. Here, Western blot data demonstrate that PMA induces cofilin dephosphorylation at Ser-3 in a time-course dependent manner (5 min–60 min) in monocytes (Suppl. Figs. 8C–D). Taken together, these results suggest that NOX2-derived $O_2^{\cdot-}$ production contributes to macropinocytosis stimulation in monocytes.

3.6. Characterization of human monocyte subsets isolated from normocholesterolemic and hypercholesterolemic patients

Human monocytes have been identified and characterized based primarily on the expression of clusters of differentiation (CD)14 and CD16 on their cell surface. Human monocytes are classified into three distinct subsets: classical ($CD14^{++}CD16^{-}$), intermediate ($CD14^{++}CD16^{+}$), and non-classical ($CD14^{+}CD16^{+}$) monocytes [40-43]. While the composition of monocyte subsets has been described in healthy individuals, the relative proportion of each group in human cardiovascular disease remains less characterized [44]. Furthermore, although the presence of lipid-laden foamy monocytes has been demonstrated in human studies, in which subset these monocytes fall into in hypercholesterolemic patients remains unknown. Subset frequencies of isolated monocytes were analyzed using peripheral blood

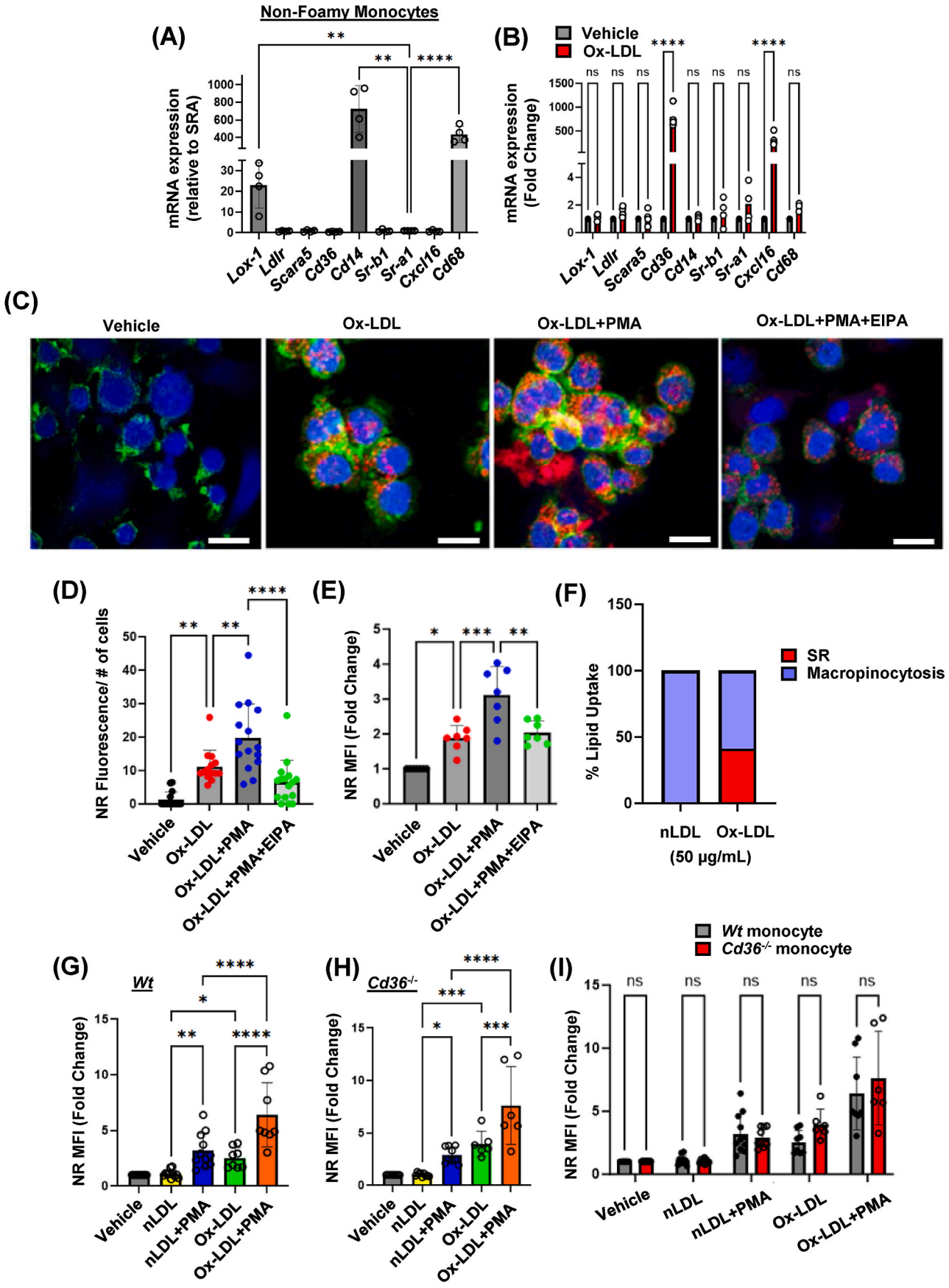

(caption on next page)

Fig. 2. Scavenger receptors and macropinocytosis contribute to ox-LDL uptake and foamy monocyte formation *in vitro*. **(A)** Scavenger receptor mRNA expression levels relative to *Sr-a1* in untreated *wild type* bone marrow-derived monocytes. ($n = 4$). **(B)** Scavenger receptor mRNA expression levels in *wild type* bone marrow monocytes treated with vehicle or ox-LDL (50 μg/mL, 24 h). ($n = 4$). **(C)** THP-1 monocytes were treated with vehicle or PMA (1 μM) ± EIPA (25 μM, 30 min pre-incubation) in the presence of ox-LDL (50 μg/mL, 24hr). Cells were fixed in 4 % PFA and nuclei stained with Hoechst (*blue*); F-actin was labeled with 488 phalloidin (*green*); and lipids were visualized using Nile Red (*red*). Images were taken with a Zeiss 780 inverted confocal microscope. Scale bar: 10 μm. **(D)** Quantification of Nile Red fluorescence normalized to the number of cells in the microscopic field of view. ($n = 3$; individual data points represent technical replicates). **(E)** THP-1 monocytes were treated as described in **(C),** stained with Nile Red and analyzed via FACS (Ex: 488 nm, Ex: 586/20 nm). ($n = 7$). **(F)** Relative contribution of scavenger receptor vs. macropinocytosis to monocyte uptake of nLDL and ox-LDL. **(G-I)** Bone marrow monocytes from *wild type* and *Cd36*$^{-/-}$ mice were treated with vehicle or PMA (1 μM) in the presence of nLDL (50 μg/mL, 24 h) or ox-LDL (50 μg/mL, 24hr). Cells were stained with Nile Red and analyzed via FACS. ($n = 6$–11). Data are presented as means ± SD. ns = not significant; *$p<0.05$; **$p<0.01$; ***$p<0.001$; ****$p<0.0001$. P values were calculated using *t*-test (A, B, I) or one way ANOVA (D, E, G, H) with Tukey's test for multiple comparisons. (For interpretation of the references to colour in this figure legend, the reader is referred to the Web version of this article.)

drawn from healthy donors and hypercholesterolemic patients via conventional flow cytometry. Donor characteristics and lipid profiles are described in Suppl. Table 3. Total plasma cholesterol, LDL cholesterol and HDL cholesterol levels were significantly elevated in hypercholesterolemic patients compared to normocholesterolemic controls (Suppl. Figs. 9F, H, J). Postprandial hypertriglyceridemia is associated with elevated levels of triglyceride-rich lipoproteins (TRL) and increased foamy monocyte formation in healthy individuals [45]. Plasma triglyceride levels were not different in hypercholesterolemic vs. normocholesterolemic individuals after overnight fasting (Suppl. Table 3, Suppl. Fig. 9G). Indirect magnetic labeling allowed simultaneous enrichment of classical, non-classical and intermediate monocytes, so that each monocyte subsets could be characterized without altering their relative frequencies. Representative gating strategy identifying isolated CD115^{+} circulating monocytes is shown in Suppl. Figs. 9K–N. Flow cytometry analysis of CD14 and CD16 expression demonstrated a significant increase in intermediate monocytes in high cholesterol patients and no changes in the relative frequencies of classical and non-classical monocytes were observed in comparison to individuals in the normal cholesterol group (Fig. 6A–E). The Fluorescence Minus One (FMO) controls for all fluorochrome-conjugated primary antibodies are shown in Suppl. Figs. 9M–P. Previous studies identified foamy monocytes by a markedly increased side scatter (SSC), which demonstrates increased granularity due to the presence of cytoplasmic lipid droplets [7,46]. Side scatter of total CD115^{+} monocytes was significantly higher in hypercholesterolemic patients compared to normocholesterolemic controls (Fig. 6F). Further analysis showed that while the SSC of classical CD14^{++}CD16^{-} monocytes from hypercholesterolemic patients was significantly higher than the SSC of classical monocytes from individuals with normal cholesterol levels, there were no differences within the intermediate and nonclassical subsets (Fig. 6G–I). Perilipin-2 is a protein that coats intracellular lipid storage droplets in foam cells [47,48]. Flow cytometry experiments confirmed that lipid-laden human monocytes with increased SSC stain positive for perilipin-2 (Fig. 6J–K). Taken together, these results suggest that monocyte subset composition is skewed towards the intermediate group in high cholesterol level individuals compared to normocholesterolemic controls. These results also demonstrate an increased percentage of foamy monocytes in the circulation of high cholesterol patients compared to normocholesterolemic individuals.

4. Discussion

Transmigration of monocytes across the endothelial layer and their differentiation into macrophages play an important role in the initiation and progression of atherosclerosis [49,50]. The classical dogma is that these monocyte-derived macrophages internalize sub-endothelially trapped oxidatively-modified LDL, become lipid-laden foam cells in the arterial wall and drive the pathogenesis of atherosclerosis [49,51]. Importantly, recent human and animal studies have demonstrated the ability of circulating monocytes in internalizing plasma lipoproteins prior to their infiltration into the arterial wall [7,8,52]. These findings have added novel information to the current concept of atherosclerosis development and have identified lipid-laden foamy monocytes as new therapeutic targets in the treatment of atherosclerosis. Despite these advances, the precise endocytic mechanisms by which monocyte lipid internalization in the circulation occurs remain unknown. Identifying these mechanisms was the central goal of this study.

Studies in both mice and humans with hypercholesterolemia have revealed the presence of foamy monocytes in the bloodstream [7,8,52-54]. In *Apoe*$^{-/-}$mice on a Western diet for 12 weeks, foamy monocytes constitute approximately 30-40 % of total monocytes [7]. Similarly, in patients with familial hypercholesterolemia (FH), foamy monocytes make up approximately 75 % of the total monocyte population [8]. In our current study, we confirmed increased numbers of circulating foamy monocytes in two separate murine models of hypercholesterolemia: *Apoe*$^{-/-}$mice and AAV8-PCSK9-induced LDLR downregulated mice. Similarly, the number of circulating foamy monocytes in hypercholesterolemic patients significantly increased compared to normocholesterolemic controls. This difference seems to be attributed to an increase in foamy monocytes within the classical monocyte subset in patients with high cholesterol levels.

While the precise mechanisms responsible for foamy monocyte formation remain unclear, previous research has identified SR CD36 as a possible endocytic mechanism responsible for monocyte LDL internalization [7,9]. CD36 is crucial for the uptake of ox-LDL in macrophages and formation of macrophage foam cells *in vitro* and in the arterial wall *in vivo* [29,55,56]. CD36 is expressed in various other cell types including endothelial cells, platelets and monocytes [57-60]. *In vitro* studies have shown that treating THP-1 monocytes with CE-VLDL increases CD36 expression and enhances its scavenger function, suggesting a positive feedback loop that promotes foamy monocyte formation [7]. These findings are supported by human data showing that foamy monocytes from hypercholesterolemic patients have increased expression of CD36 [61]. Despite these findings, *Cd36*$^{-/-}$ mice are only partially protected from atherosclerosis [10-12] and there is only a partial (~30 %) decrease of circulating foamy monocytes in *Cd36*$^{-/-}$ mice suggesting that CD36 -independent endocytic mechanisms may also contribute to foamy monocyte formation *in vivo*.

In the present study, we found low levels of *Cd36* mRNA expression in monocytes isolated from normocholesterolemic *wild type* mice. Scavenger receptors *Lox-1*, *Cd68*, and *Cd14* showed significantly higher mRNA expression in monocytes compared to *Cd36* and *Sr-a1*. Ox-LDL uptake was not inhibited in *Cd36*$^{-/-}$ monocytes *in vitro*, consistent with low CD36 expression in non-foamy monocytes. We speculate that LOX-1, CD68, and CD14 may be responsible for ox-LDL uptake in *wild type* monocytes isolated from normocholesterolemic control mice. Interestingly, ox-LDL treatment of monocytes significantly increased *Cd36* mRNA expression, suggesting a role for CD36 in lipoprotein uptake after foamy monocyte formation has begun. Our results demonstrated that foamy monocyte formation decreased in hypercholesterolemic *Cd36*$^{-/-}$ mice.

Macropinocytosis is a highly conserved, actin-dependent endocytic process by which extracellular fluid and pericellular solutes (*e.g.* LDL) are internalized into cells [16]. Macropinocytosis is a unique form of endocytosis as pericellular solutes do not require physical or specific

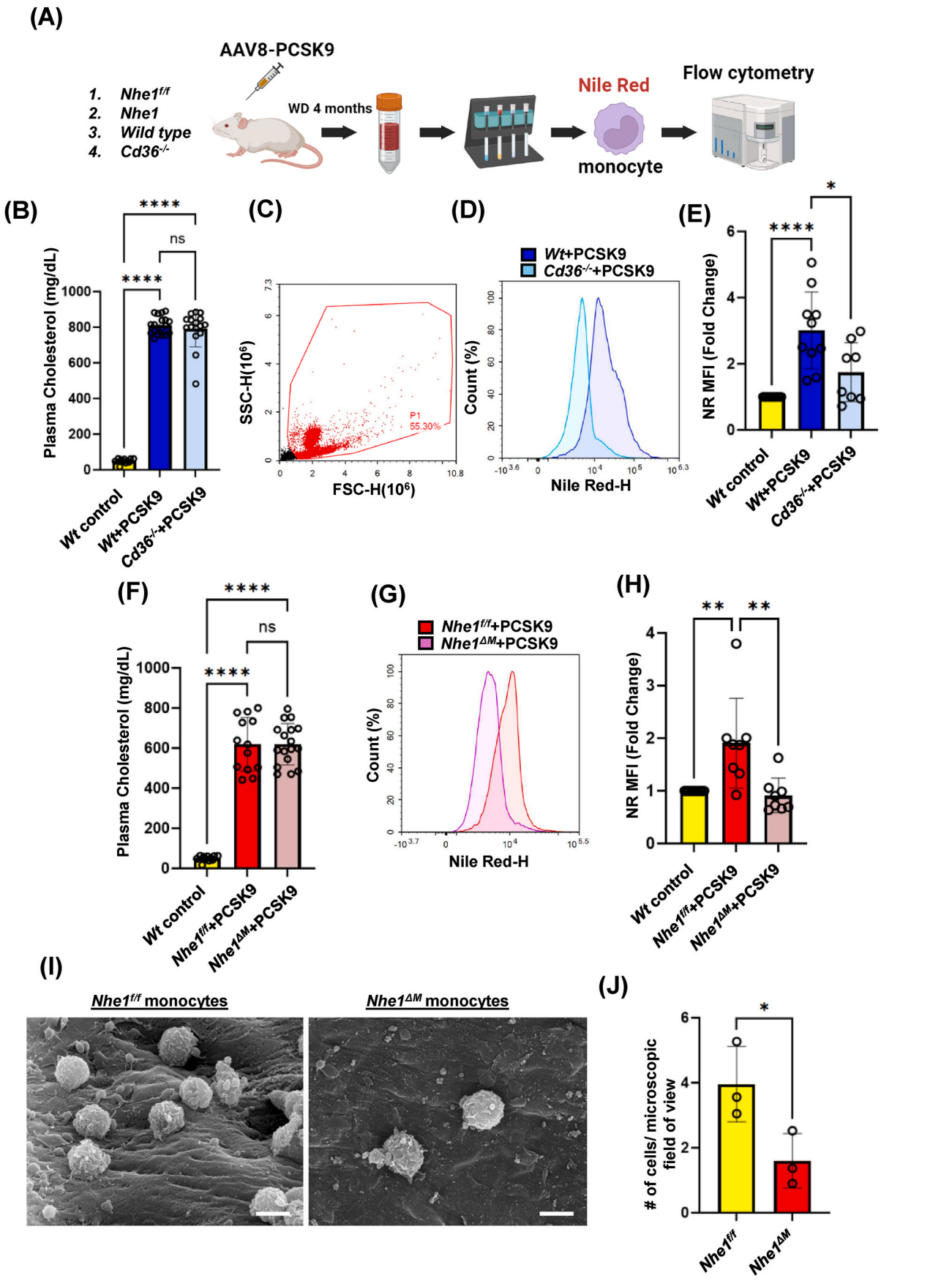

(caption on next page)

Fig. 3. Macropinocytosis and CD36 mediate lipid uptake and promote foamy monocyte formation in hypercholesterolemic mice *in vivo*. **(A)** Schematic flow chart of experimental design. **(B)** Total plasma cholesterol of normocholesterolemic *wild type* and hypercholesterolemic *wild type* and *Cd36*$^{-/-}$ mice. ($n = 11$–19). **(C)** Flow cytometry gating strategy. **(D, E)** Quantification of Nile Red fluorescent intensity in circulating monocytes isolated from mice described in **(B)**. ($n = 8$–10). **(F)** Total plasma cholesterol levels of control *wild type* and hypercholesterolemic *Nhe1*$^{f/f}$, and *Nhe1*$^{\Delta M}$ mice. ($n = 13$–17). **(G, H)** Quantification of Nile Red fluorescent intensity in circulating monocytes isolated from mice described in **(F)**. ($n = 8$–10). **(I)** Representative SEM images showing monocyte adhesion to the inner curvature of atherosclerotic aorta *ex vivo*. Scale bar: 5 μm. **(J)** Quantification of the number of adhered monocytes per microscopic field of view. Data are presented as means ± SD. ns = not significant; *$p<0.05$; **$p<0.01$; ****$p<0.0001$. P values were calculated using *t*-test (J) or one-way ANOVA (B, E, F, H) with Tukey's test for multiple comparisons. (For interpretation of the references to colour in this figure legend, the reader is referred to the Web version of this article.)

interaction with the plasma membrane (ie: receptor binding) to be internalized. Consequently, solute or LDL internalization by macropinocytosis is a receptor-independent endocytic process [18]. Previous studies by Kruth et al. and others demonstrated that stimulation of macropinocytosis in macrophages increases nLDL internalization, leading to foam cell formation *in vitro* [17,19]. To our knowledge, the role of macropinocytosis in monocyte LDL internalization and foam cell formation *in vitro* or in hypercholesterolemic mice *in vivo* has not been investigated.

In vitro experiments using scanning electron microscopy, flow cytometry analysis, and confocal imaging demonstrated that monocytes stimulated with phorbol 12-myristate 13-acetate (PMA) - the current gold standard, non-physiological stimulator of macropinocytosis [21] - exhibit membrane ruffling and significantly increased internalization of nLDL, leading to the formation of lipid-laden foamy monocytes. The amiloride derivative 5-(N-Ethyl-N-isopropyl) amiloride (EIPA) - a well-established inhibitor of macropinocytosis [62] - abolished PMA-induced membrane ruffling and foamy monocyte formation. It is important to note that in addition to stimulating macropinocytosis, PMA also induces monocyte to macrophage differentiation. However, this process occurs over 3 to 5 days [63,64], a time frame well outside of our macropinocytosis experiments. Interestingly, ox-LDL treatment (50 μg/mL, 24 h) alone did not induce monocyte to macrophage differentiation as determined by MERTK protein expression. While this finding appears to contradict previous studies that indicate ox-LDL or its components can promote monocyte differentiation into macrophages [65-67], it is difficult to draw definitive conclusions. Each study employed different monocytic cell lines or primary cells, utilized varied time points, and assessed distinct markers for differentiation. This variability complicates efforts to determine the precise effects and timeline of lipid-induced differentiation. The relatively low concentrations of nLDL (50 μg/ml) that we used indicate that macropinocytosis-mediated foamy monocyte formation may occur even in individuals with normal or low LDL concentrations if monocyte macropinocytosis is stimulated. Interestingly, previous studies demonstrated circulating foamy monocytes in the blood of normocholesterolemic individuals [8].

Stimulation of macropinocytosis in the presence of ox-LDL resulted in a notable increase in foamy monocyte formation when compared with either macropinocytosis- or scavenger receptor-mediated pathways alone in both murine and human THP-1 monocytes. These results suggest an additive effect between these two endocytic processes leading to lipid uptake. Further analysis demonstrated that while macropinocytosis contributes to ~60 % of lipid internalization when ox-LDL is present, macropinocytosis was found to be responsible for all lipid uptake in the presence of nLDL. These results confirm findings from previous studies which demonstrate that SR exhibit very little affinity for nLDL [14,15]. The importance of macropinocytosis in foamy monocyte formation *in vivo* may be further amplified when taking into consideration that ox-LDL represents a relatively small proportion of plasma LDL in dyslipidemic patients [13].

Our lab has previously demonstrated that genetic inhibition of macropinocytosis in myeloid cells (*Nhe1*$^{\Delta M}$) inhibits macrophage macropinocytosis and significantly decreases atherosclerosis lesion development [19]. Previous studies have reported NHE1 as the most highly expressed NHE isoform in monocytes [68]. Inhibition of NHE1 has been demonstrated to suppress actin polymerization and membrane ruffle formation during macropinocytosis by regulating the cytosolic pH just beneath the plasma membrane [27]. In the current study, we utilized hypercholesterolemic *Nhe1*$^{\Delta M}$ mice to genetically inhibit macropinocytosis in monocytes and found a significant (~50 %) reduction in foamy monocyte formation when compared to *Nhe1*$^{f/f}$ controls. A similar decrease was found in hypercholesterolemic *Cd36*$^{-/-}$ mice when compared to *wild type* controls, suggesting that both macropinocytosis and CD36 contribute to foamy monocyte formation *in vivo*.

The functional relevance of foamy monocytes in atherosclerosis development has been documented by several groups. In hypercholesterolemic mice and humans, upregulation of CD11c, a β_2 integrin on foamy monocytes, was found to be necessary for adhesion to the diseased endothelium [7]. Deletion of murine CD11c decreased foamy monocyte adhesion and transmigration into the arterial wall and inhibited atherosclerotic lesion development [69]. Another study demonstrated the upregulation of chemokine receptor type 2 (CCR2) in foamy monocytes, which promoted enhanced migration capacity of these cells [8]. Our bulk RNA-sequencing results demonstrated that the majority of chemokine ligand (~80 %) and chemokine receptor (~55 %) related genes were upregulated in monocytes compared to macrophages regardless of lipid status, confirming the notion that these molecules play important roles in directing monocyte traffic. Interestingly, gene expressions for chemokines *Ccl7*, *Ccl9*, and *Ccl19*, as well as chemokine receptor *Ccr3* were significantly increased in foamy monocytes compared to foamy macrophages but were not different between untreated cells, suggesting that these ligand-receptor proteins may act as selective therapeutic targets for preventing cholesterol accumulation in atherosclerosis.

In our current study, circulating monocytes from macropinocytosis-deficient *Nhe1*$^{\Delta M}$ mice adhered to an atherosclerotic aorta at a substantially (~60 %) lower degree *ex vivo* when compared to foamy monocytes from control mice. These SEM imaging and quantification results support the notion that macropinocytosis-mediated lipid accumulation in monocytes changes their phenotypic and functional properties leading to increased endothelial cell adhesion and accelerated atherosclerosis development.

NADPH oxidase 2 (NOX2) is a multi-component enzyme that consists of plasma membrane-bound NOX2 and p22^{phox} as well as cytoplasmic subunits p47^{phox}, p67^{phox} and RAC1 [70]. Upon activation, p47^{phox}, p67^{phox} and Rac1 translocate to NOX2 and p22^{phox}. The cytosolic subunit Rac1 then promotes activation and binding of the p67^{phox} - p47^{phox} complex to the catalytic core of the enzyme, which stimulates its activity leading to superoxide anion (O_2^-) production [37]. NOX2 localizes to both intracellular and plasma membranes in phagocytes [70]. This localization underpins the idea of compartmentalization in ROS-mediated signaling and function. ROS produced within cytosolic compartments activate redox-sensitive signaling pathways [71], while NOX2 in the plasma membrane contributes to intercellular ROS-mediated signaling [72]. PMA mimics endogenously produced diacylglycerol (DAG) and stimulates PKC activation in both macrophages and nonphagocytic cells [37,73,74]. Direct stimulation of PKC by PMA phosphorylates the NOX organizer subunit p47^{phox} in macrophages, leading to enzymatic assembly of NOX2 and subsequent O_2^- generation. The resulting O_2^- production signals downstream to activate actin regulator cofilin, leading to membrane ruffle formation and macropinocytotic internalization of extracellular fluid and solute in macrophages [37]. The activity of cofilin is increased when it is

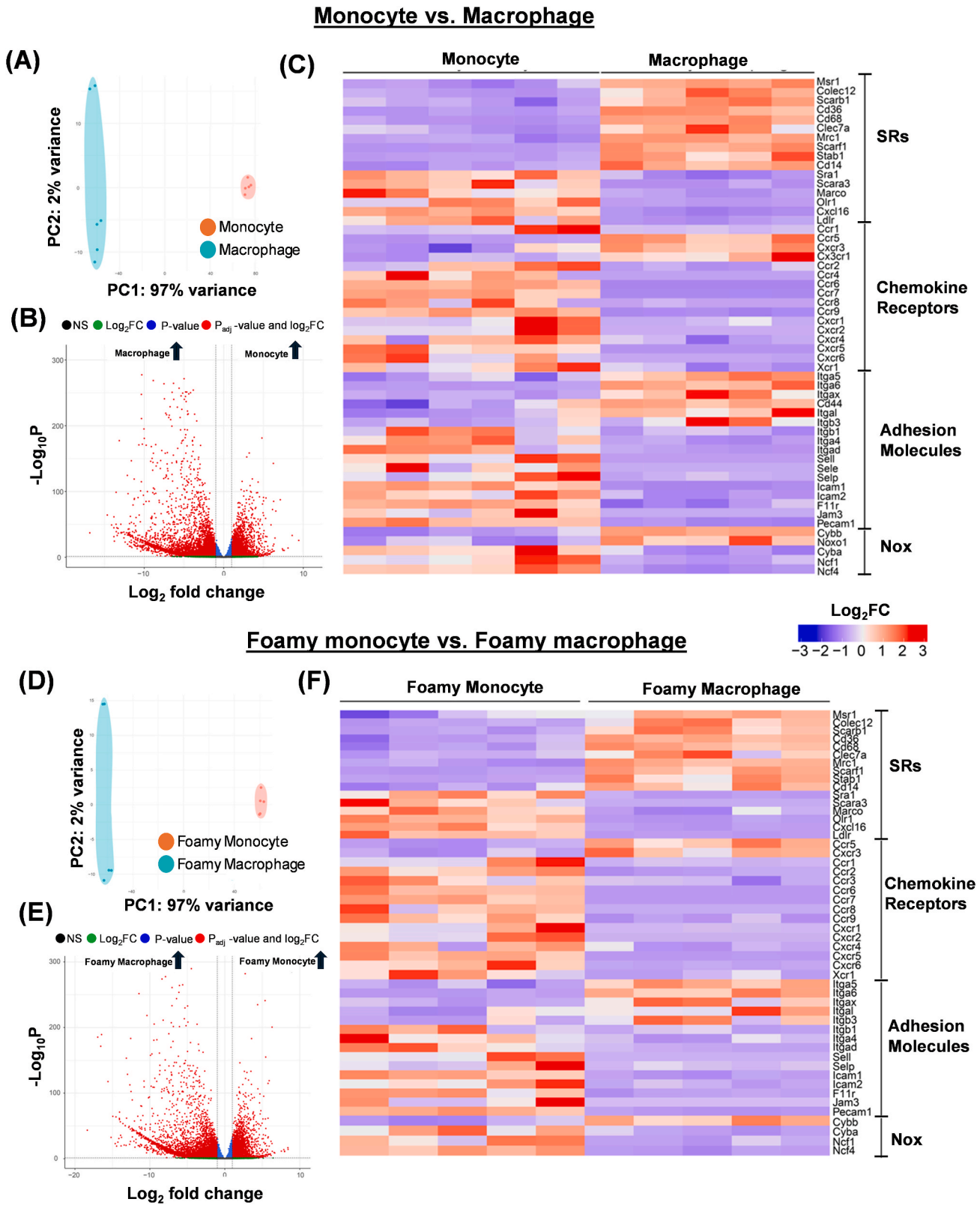

Fig. 4. Gene expression in foamy and non-foamy monocytes and macrophages. (A) Principal component analysis (PCA) for *wild type* splenic monocytes and splenic monocyte-derived macrophages. ($n = 5$–6 per group). **(B)** Volcano plot for bulk RNA sequencing from samples shown in **(A)**. **(C)** Heatmap for the expressions of genes for scavenger receptors (SR), chemokine receptors, adhesion molecules, and NOX subunits from bulk RNA sequencing in **(A-B)**. **(D)** PCA for *wild type* splenic monocytes and splenic monocyte-derived macrophages treated with ox-LDL (50 μg/mL, 24 h). ($n = 5$ per group). **(E)** Volcano plot for bulk RNA sequencing from samples shown in **(D)**. **(F)** Heatmap for the expressions of genes for SRs, chemokine receptors, adhesion molecules, and NOX subunits of foamy monocytes and foamy macrophages from bulk RNA sequencing in **(D-E)**. Significance was determined with a p-adjusted value of <0.05.

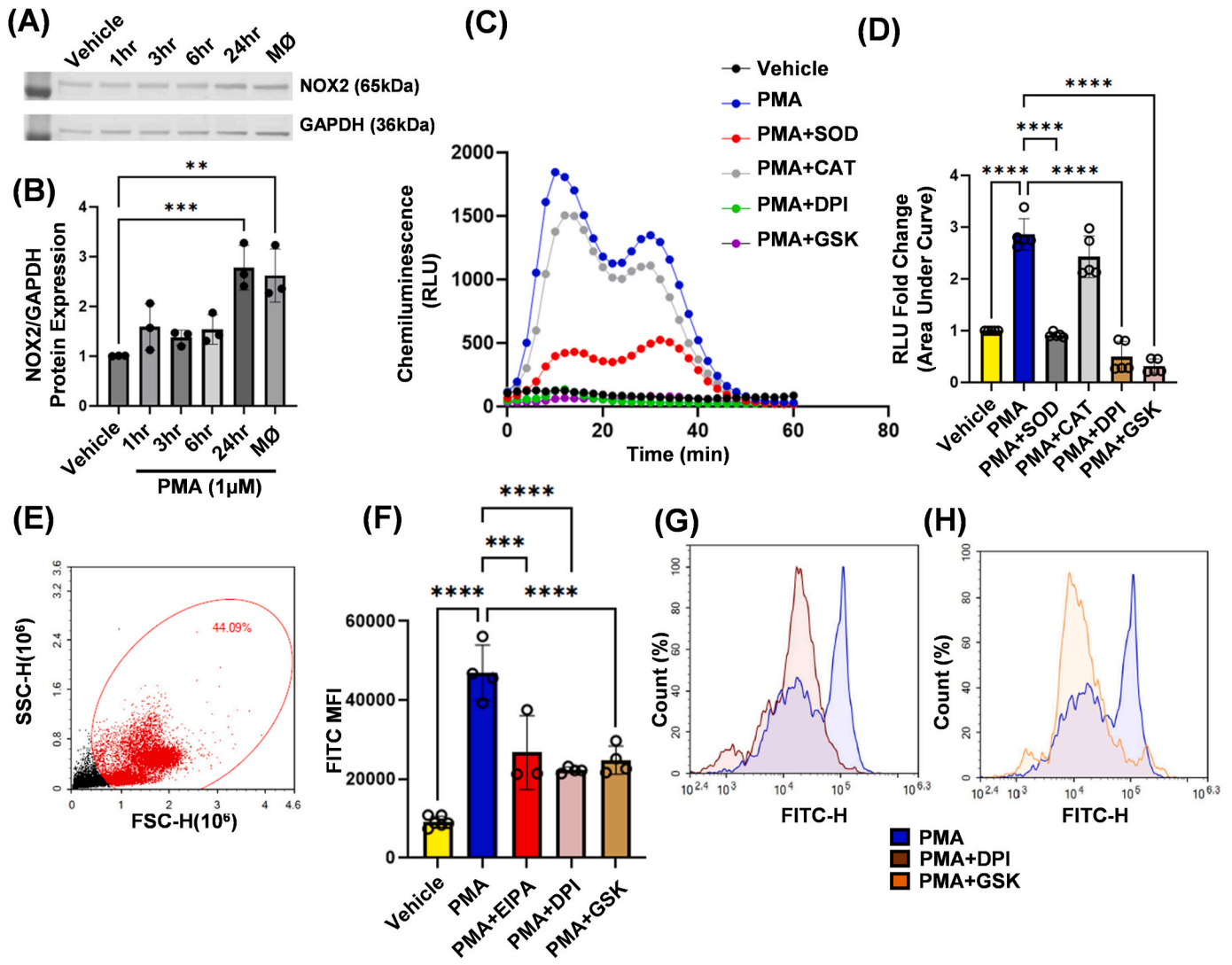

Fig. 5. Increased NADPH Oxidase 2 (NOX2) activity stimulates macropinocytosis in monocytes. (A) THP-1 monocytes were treated with either vehicle or PMA (1 μM, 1 h–24 h). Positive control macrophages (MØ): 1 μM PMA for 7 days. Lysates were subjected to Western blot analysis for NOX2. Representative Western blot image is shown. **(B)** Quantification of NOX2 protein expression normalized to GAPDH. *(n = 3)*. **(C, D)** *Wild type* splenic monocytes were treated with vehicle or PMA (1 μM, 3 h), ± DPI (5 μM, 30 min preincubation) or GSK2795039 (20 μM, 30 min preincubation) and $O_2^{\cdot-}$ production was monitored via L-012 chemiluminescence. Representative chemiluminescence signal curves are shown. SOD and CAT were used as antioxidant controls *(n = 5)*. **(E)** Representative flow cytometry gating strategy. **(F–H)** FITC-dextran uptake after treatment as indicated in **(C, D)**. *(n = 3-5)*. Data are presented as means ± SD. $^{**}p<0.01$; $^{***}p<0.001$; $^{****}p<0.0001$. P values were calculated using one-way ANOVA with Tukey's test for multiple comparisons.

dephosphorylated at Ser-3 [37]. Whether this mechanism holds true for monocytes is currently unknown. Immunoblotting experiments demonstrated that monocytes express NOX2. Chemiluminescent detection of monocyte-derived $O_2^{\cdot-}$ was confirmed by superoxide dismutase (SOD) [75,76]. Both DPI, a nonspecific small molecule inhibitor of flavin-containing oxidases [77], and GSK2795039, a specific small molecule inhibitor of NOX2 [39], significantly decreased PMA-induced $O_2^{\cdot-}$ production in monocytes. Flow cytometry experiments demonstrated that DPI and GSK2795039 inhibited macropinocytosis stimulation in monocytes. Western blot analysis revealed that PMA treatment of monocytes induced Ser-3 dephosphorylation of cofilin. Taken together, these results suggest that NOX2-derived $O_2^{\cdot-}$ production and activation of cofilin contribute to macropinocytosis stimulation in monocytes. One limitation of this study is that we did not explore the role of NOX2 *in vivo*. While previous research has indicated that ROS levels are increased in circulating monocytes of hypercholesterolemic mice [78] and that NOX2 knockout mice exhibit protection against atherosclerosis [79,80], it remains unclear whether $O_2^{\cdot-}$ production is necessary to stimulate monocyte macropinocytosis leading to foamy monocyte formation *in vivo*.

Human monocytes are categorized into three distinct subsets based on the expression levels of cell surface markers CD14 and CD16: classical $CD14^{++}CD16^{-}$, nonclassical $CD14^{+}CD16^{+}$ and intermediate $CD14^{+}CD16^{+}$ monocytes [40-42]. The roles and functions of each monocyte subset in atherosclerosis is not fully understood but in general, classical monocytes have been shown to act as inflammatory mediators and preferentially infiltrate across the arterial endothelium, while nonclassical monocytes serve to patrol the arterial wall and maintain vascular tissue homeostasis [81-83]. Recent fate-mapping studies have shown that the nonclassical subset arises from circulating classical monocytes via the intermediate subset- a transitional group that exhibits functional characteristics of both classical and nonclassical monocytes [84]. The dynamic transition between monocyte subsets is a critical aspect of the immune response that plays a significant role in atherosclerosis development.

The relative proportion of each monocyte subset varies based on the physiological conditions, health status, and disease state of the individual. Studies using murine models of hypercholesterolemia have

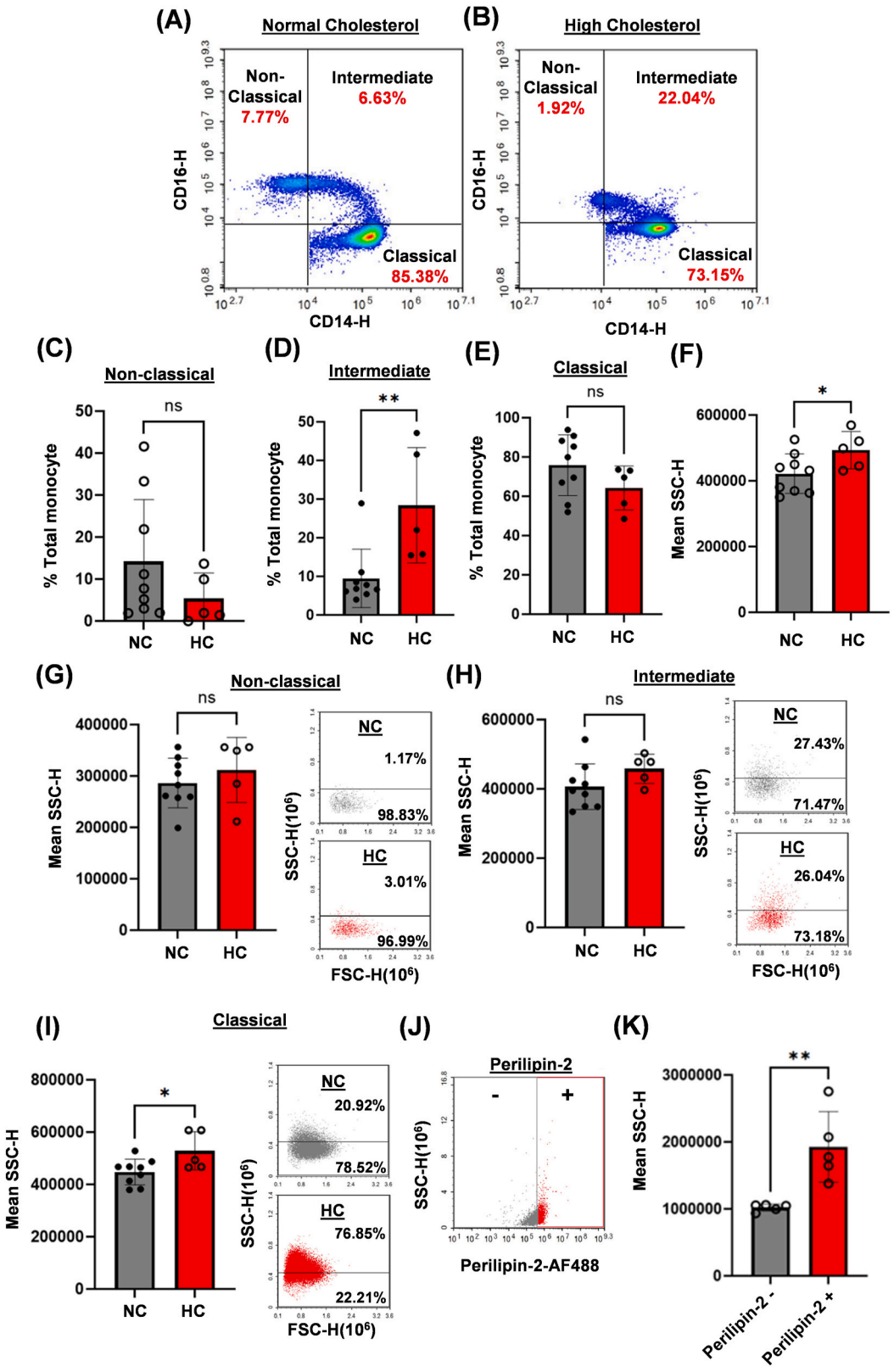

Fig. 6. Characterization of human monocyte subsets isolated from normocholesterolemic controls and hypercholesterolemic patients. (A-B) Representative flow cytometry density plots indicating relative frequencies of CD14 and CD16 expression in circulating monocytes from normocholesterolemic controls (NC) and high cholesterol (HC) patients. Results from flow cytometry experiments show relative percentage of **(C)** nonclassical monocytes, **(D)** intermediate monocytes, and **(E)** classical monocytes. *(n = 5–9)*. **(F)** Side scatter (SSC) of total CD115^{+} monocytes between groups. *(n = 5–9)*. Further analysis comparing SSC of nonclassical **(G)** intermediate **(H)** and classical **(I)** monocytes between groups. *(n = 5–9)*. **(J, K)** Flow cytometry quantification of SSC in peripilin-2^{+} and perilipin-2^{-} THP-1 monocytes. *(n = 5)*. Data are presented as means ± SD. *$p<0.05$; **$p<0.005$. P values were calculated using *t*-test.

demonstrated increased prevalence of circulating classical monocytes and decreased levels of nonclassical monocytes [81,82]. Meanwhile, studies in humans have shown elevated classical monocyte levels in acute myocardial infarction and heart failure patients [85,86]. While these results suggest a strong correlation between increased classical monocyte numbers and cardiovascular disease outcome, the research remains controversial. For example, a large clinical study of patients undergoing coronary angiography demonstrated an association between increased intermediate monocytes and predicted cardiovascular death [87]. Other human studies of hyperlipidemia demonstrated a significant association between increased number of intermediate monocytes and atherosclerosis [88-90]. Consistent with these latter reports, our data show a significantly increased intermediate monocyte population but no significant difference within the classical or nonclassical monocyte subsets in hypercholesterolemic patients when compared to healthy controls. These results suggest that in high cholesterol conditions, monocytes respond to heightened inflammation and differentiate into the intermediate phenotype. Their further development into anti-inflammatory, tissue-repairing nonclassical monocytes may be impaired, which may ultimately enhance overall disease progression. It is important to recognize that this dynamic spectrum of monocyte phenotypes complicates accurate classification using flow cytometry gating approaches and is a limitation of our study [91,92]. An additional complicating issue is that monocyte heterogeneity can be influenced by multiple factors beyond plasma cholesterol, including sex [93], ethnicity [94], age [93], body weight [95], sleep patterns [96], and exercise [97]. These variables can affect the donor's plasma microenvironment and may partly explain the subtle variations in CD14 and CD16 expression that we observed between groups.

5. Conclusion

In conclusion, our results support an important role for monocyte macropinocytosis in plasma LDL uptake in hypercholesterolemic conditions. Data from multiple imaging and flow cytometry experiments demonstrated for the first time that receptor-independent macropinocytosis of lipoproteins leads to the formation of lipid-laden foamy monocytes *in vitro* and *in vivo*. Given that macropinocytosis of nLDL is linearly related to extracellular lipid concentration and that ox-LDL represents a relatively small fraction of total circulating LDL, our findings emphasize the importance of macropinocytosis relative to the SR-CD36-mediated pathway in foamy monocyte formation. Mechanistically, we demonstrate that monocyte macropinocytosis is regulated by NOX2 activity with $O_2^{\cdot-}$ serving as the downstream signaling molecule leading to membrane ruffling and solute internalization. Data from our primary human monocyte experiments confirm previous reports of elevated foamy monocyte levels in high cholesterol patients and overall increases in the intermediate monocyte subset. In summary, our results highlight monocyte macropinocytosis as a new mechanism of foam cell formation and identifies this pathway as an alternative therapeutic target for combating atherosclerosis.

CRediT authorship contribution statement

WonMo Ahn: Writing – review & editing, Writing – original draft, Visualization, Validation, Supervision, Software, Resources, Project administration, Methodology, Investigation, Funding acquisition, Formal analysis, Data curation, Conceptualization. **Faith N. Burnett:** Writing – review & editing, Visualization, Validation, Supervision, Software, Resources, Project administration, Methodology, Investigation, Formal analysis, Data curation, Conceptualization. **Kamila Wojnar-Lason:** Methodology, Data curation. **Jaser Doja:** Software, Formal analysis. **Amritha Sreekumar:** Data curation. **Pushpankur Ghoshal:** Supervision, Data curation. **Bhupesh Singla:** Supervision, Funding acquisition, Data curation. **Graydon Gonsalvez:** Supervision, Methodology. **Ryan A. Harris:** Supervision, Resources, Funding acquisition. **Xiaoling Wang:** Supervision, Funding acquisition. **Joseph M. Miano:** Investigation, Conceptualization. **Gábor Csányi:** Writing – review & editing, Writing – original draft, Visualization, Validation, Supervision, Software, Resources, Project administration, Methodology, Investigation, Funding acquisition, Formal analysis, Data curation, Conceptualization.

Sources of funding

This work was supported by the National Institutes of Health grants 5R01HL139562-05, 5R00HL114648-05, 5R00HL146954-05 and 5R01HL164792-02 awarded to GC, 5K99HL146954-02 and 5R00HL146954-05 awarded to BS, 5F31HL162498-03 awarded to WA, and 5R01DK117365-05 awarded to RAH and XW, and the American Heart Association grants 23TPA1141161 awarded to GC, and SFRN863621 awarded to RAH.

Declaration of competing interest

The authors declare that the research was conducted in the absence of any commercial or financial relationships that could be taken as a potential conflict of interest.

Acknowledgement

The authors would like to thank Libby Perry and Brendan Marshall (Augusta University) for their help with the SEM imaging experiments. We thank the Medical Illustration Department (Augusta University) for providing the graphical abstract. We thank William Bryant of the Vascular Biology Center at Augusta University for his help analyzing the Bulk RNA-sequencing data. We thank the Genome Technology Access Center at the McDonnell Genome Institute at Washington University School of Medicine for their help with genomic analysis. The Center is partially supported by NCI Cancer Center Support Grant #P30 CA91842 to the Siteman Cancer Center. This publication is solely the responsibility of the authors and does not necessarily represent the official view of NCRR or NIH.

Appendix A. Supplementary data

Supplementary data to this article can be found online at https://doi.org/10.1016/j.redox.2024.103423.

Data availability

Data will be made available on request.

References

[1] W. Herrington, B. Lacey, P. Sherliker, J. Armitage, S. Lewington, Epidemiology of atherosclerosis and the potential to reduce the global burden of atherothrombotic disease, Circ. Res. 118 (2016) 535–546, https://doi.org/10.1161/CIRCRESAHA.115.307611.

[2] X.H. Yu, Y.C. Fu, D.W. Zhang, K. Yin, C.K. Tang, Foam cells in atherosclerosis, Clin. Chim. Acta 424 (2013) 245–252, https://doi.org/10.1016/j.cca.2013.06.006.

[3] Y. Gui, H. Zheng, R.Y. Cao, Foam cells in atherosclerosis: novel insights into its origins, consequences, and molecular mechanisms, Front Cardiovasc Med 9 (2022) 845942, https://doi.org/10.3389/fcvm.2022.845942.

[4] S. Ghosh, B. Zhao, J. Bie, J. Song, Macrophage cholesteryl ester mobilization and atherosclerosis, Vasc. Pharmacol. 52 (2010) 1–10, https://doi.org/10.1016/j.vph.2009.10.002.

[5] M.G. Silverman, B.A. Ference, K. Im, S.D. Wiviott, R.P. Giugliano, S.M. Grundy, E. Braunwald, M.S. Sabatine, Association between lowering LDL-C and cardiovascular risk reduction among different therapeutic interventions: a systematic review and meta-analysis, JAMA 316 (2016) 1289–1297, https://doi.org/10.1001/jama.2016.13985.

[6] D. Lloyd-Jones, R. Adams, M. Carnethon, G. De Simone, T.B. Ferguson, K. Flegal, E. Ford, K. Furie, A. Go, K. Greenlund, et al., Heart disease and stroke statistics–2009 update: a report from the American heart association statistics committee and stroke statistics subcommittee, Circulation 119 (2009) 480–486, https://doi.org/10.1161/CIRCULATIONAHA.108.191259.

[7] L. Xu, X. Dai Perrard, J.L. Perrard, D. Yang, X. Xiao, B.B. Teng, S.I. Simon, C. M. Ballantyne, H. Wu, Foamy monocytes form early and contribute to nascent atherosclerosis in mice with hypercholesterolemia, Arterioscler. Thromb. Vasc. Biol. 35 (2015) 1787–1797, https://doi.org/10.1161/ATVBAHA.115.305609.

[8] S.J. Bernelot Moens, A.E. Neele, J. Kroon, F.M. van der Valk, J. Van den Bossche, M.A. Hoeksema, R.M. Hoogeveen, J.G. Schnitzler, M.T. Baccara-Dinet, G. Manvelian, et al., PCSK9 monoclonal antibodies reverse the pro-inflammatory profile of monocytes in familial hypercholesterolaemia, Eur. Heart J. 38 (2017) 1584–1593, https://doi.org/10.1093/eurheartj/ehx002.

[9] Y. Chen, J. Zhang, W. Cui, R.L. Silverstein, CD36, a signaling receptor and fatty acid transporter that regulates immune cell metabolism and fate, J. Exp. Med. 219 (2022), https://doi.org/10.1084/jem.20211314.

[10] S. Kuchibhotla, D. Vanegas, D.J. Kennedy, E. Guy, G. Nimako, R.E. Morton, M. Febbraio, Absence of CD36 protects against atherosclerosis in ApoE knock-out mice with no additional protection provided by absence of scavenger receptor A I/II, Cardiovasc. Res. 78 (2008) 185–196, https://doi.org/10.1093/cvr/cvm093.

[11] K.J. Moore, V.V. Kunjathoor, S.L. Koehn, J.J. Manning, A.A. Tseng, J.M. Silver, M. McKee, M.W. Freeman, Loss of receptor-mediated lipid uptake via scavenger receptor A or CD36 pathways does not ameliorate atherosclerosis in hyperlipidemic mice, J. Clin. Invest. 115 (2005) 2192–2201, https://doi.org/10.1172/JCI24061.

[12] J.J. Manning-Tobin, K.J. Moore, T.A. Seimon, S.A. Bell, M. Sharuk, J.I. Alvarez-Leite, M.P. de Winther, I. Tabas, M.W. Freeman, Loss of SR-A and CD36 activity reduces atherosclerotic lesion complexity without abrogating foam cell formation in hyperlipidemic mice, Arterioscler. Thromb. Vasc. Biol. 29 (2009) 19–26, https://doi.org/10.1161/ATVBAHA.108.176644.

[13] H. Huang, W. Mai, D. Liu, Y. Hao, J. Tao, Y. Dong, The oxidation ratio of LDL: a predictor for coronary artery disease, Dis. Markers 24 (2008) 341–349, https://doi.org/10.1155/2008/371314.

[14] B. Chellan, C.A. Reardon, G.S. Getz, M.A. Hofmann Bowman, Enzymatically modified low-density lipoprotein promotes foam cell formation in smooth muscle cells via macropinocytosis and enhances receptor-mediated uptake of oxidized low-density lipoprotein, Arterioscler. Thromb. Vasc. Biol. 36 (2016) 1101–1113, https://doi.org/10.1161/ATVBAHA.116.307306.

[15] J.L. Goldstein, Y.K. Ho, S.K. Basu, M.S. Brown, Binding site on macrophages that mediates uptake and degradation of acetylated low density lipoprotein, producing massive cholesterol deposition, Proc. Natl. Acad. Sci. U.S.A. 76 (1979) 333–337, https://doi.org/10.1073/pnas.76.1.333.

[16] F. Sallusto, M. Cella, C. Danieli, A. Lanzavecchia, Dendritic cells use macropinocytosis and the mannose receptor to concentrate macromolecules in the major histocompatibility complex class II compartment: downregulation by cytokines and bacterial products, J. Exp. Med. 182 (1995) 389–400, https://doi.org/10.1084/jem.182.2.389.

[17] H.S. Kruth, N.L. Jones, W. Huang, B. Zhao, I. Ishii, J. Chang, C.A. Combs, D. Malide, W.Y. Zhang, Macropinocytosis is the endocytic pathway that mediates macrophage foam cell formation with native low density lipoprotein, J. Biol. Chem. 280 (2005) 2352–2360, https://doi.org/10.1074/jbc.M407167200.

[18] H.S. Kruth, Receptor-independent fluid-phase pinocytosis mechanisms for induction of foam cell formation with native low-density lipoprotein particles, Curr. Opin. Lipidol. 22 (2011) 386–393, https://doi.org/10.1097/MOL.0b013e32834adadb.

[19] H.P. Lin, B. Singla, W. Ahn, P. Ghoshal, M. Blahove, M. Cherian-Shaw, A. Chen, A. Haller, D.Y. Hui, K. Dong, et al., Receptor-independent fluid-phase macropinocytosis promotes arterial foam cell formation and atherosclerosis, Sci. Transl. Med. 14 (2022) eadd2376, https://doi.org/10.1126/scitranslmed.add2376.

[20] S. Bosedasgupta, J. Pieters, Inflammatory stimuli reprogram macrophage phagocytosis to macropinocytosis for the rapid elimination of pathogens, PLoS Pathog. 10 (2014) e1003879, https://doi.org/10.1371/journal.ppat.1003879.

[21] J.A. Swanson, Phorbol esters stimulate macropinocytosis and solute flow through macrophages, J. Cell Sci. 94 (Pt 1) (1989) 135–142, https://doi.org/10.1242/jcs.94.1.135.

[22] J.P. Lim, P.A. Gleeson, Macropinocytosis: an endocytic pathway for internalising large gulps, Immunol. Cell Biol. 89 (2011) 836–843, https://doi.org/10.1038/icb.2011.20.

[23] S. Wennstrom, P. Hawkins, F. Cooke, K. Hara, K. Yonezawa, M. Kasuga, T. Jackson, L. Claesson-Welsh, L. Stephens, Activation of phosphoinositide 3-kinase is required for PDGF-stimulated membrane ruffling, Curr. Biol. 4 (1994) 385–393, https://doi.org/10.1016/s0960-9822(00)00087-7.

[24] S.E. Quinn, L. Huang, J.G. Kerkvliet, J.A. Swanson, S. Smith, A.D. Hoppe, R. B. Anderson, N.W. Thiex, B.L. Scott, The structural dynamics of macropinosome formation and PI3-kinase-mediated sealing revealed by lattice light sheet microscopy, Nat. Commun. 12 (2021) 4838, https://doi.org/10.1038/s41467-021-25187-1.

[25] C.M. Buckley, H. Pots, A. Gueho, J.H. Vines, C.J. Munn, B.A. Phillips, B. Gilsbach, D. Traynor, A. Nikolaev, T. Soldati, et al., Coordinated ras and rac activity shapes macropinocytic cups and enables phagocytosis of geometrically diverse bacteria, Curr. Biol. 30 (2020) 2912–2926, https://doi.org/10.1016/j.cub.2020.05.049.

[26] G. Zizzo, B.A. Hilliard, M. Monestier, P.L. Cohen, Efficient clearance of early apoptotic cells by human macrophages requires M2c polarization and MerTK induction, J. Immunol. 189 (2012) 3508–3520, https://doi.org/10.4049/jimmunol.1200662.

[27] M. Koivusalo, C. Welch, H. Hayashi, C.C. Scott, M. Kim, T. Alexander, N. Touret, K. M. Hahn, S. Grinstein, Amiloride inhibits macropinocytosis by lowering submembranous pH and preventing Rac1 and Cdc42 signaling, J. Cell Biol. 188 (2010) 547–563, https://doi.org/10.1083/jcb.200908086.

[28] T. Kiyanagi, K. Iwabuchi, K. Shimada, K. Hirose, T. Miyazaki, K. Sumiyoshi, C. Iwahara, H. Nakayama, H. Masuda, H. Mokuno, et al., Involvement of cholesterol-enriched microdomains in class A scavenger receptor-mediated responses in human macrophages, Atherosclerosis 215 (2011) 60–69, https://doi.org/10.1016/j.atherosclerosis.2010.10.019.

[29] M. Febbraio, E.A. Podrez, J.D. Smith, D.P. Hajjar, S.L. Hazen, H.F. Hoff, K. Sharma, R.L. Silverstein, Targeted disruption of the class B scavenger receptor CD36 protects against atherosclerotic lesion development in mice, J. Clin. Invest. 105 (2000) 1049–1056, https://doi.org/10.1172/JCI9259.

[30] V.V. Kunjathoor, M. Febbraio, E.A. Podrez, K.J. Moore, L. Andersson, S. Koehn, J. S. Rhee, R. Silverstein, H.F. Hoff, M.W. Freeman, Scavenger receptors class A-I/II and CD36 are the principal receptors responsible for the uptake of modified low density lipoprotein leading to lipid loading in macrophages, J. Biol. Chem. 277 (2002) 49982–49988, https://doi.org/10.1074/jbc.M209649200.

[31] A. Alquraini, J. El Khoury, Scavenger receptors, Curr. Biol. 30 (2020) R790–R795, https://doi.org/10.1016/j.cub.2020.05.051.

[32] L. Rohrer, M. Freeman, T. Kodama, M. Penman, M. Krieger, Coiled-coil fibrous domains mediate ligand binding by macrophage scavenger receptor type II, Nature 343 (1990) 570–572, https://doi.org/10.1038/343570a0.

[33] M. Roche-Molina, D. Sanz-Rosa, F.M. Cruz, J. Garcia-Prieto, S. Lopez, R. Abia, F. J. Muriana, V. Fuster, B. Ibanez, J.A. Bernal, Induction of sustained hypercholesterolemia by single adeno-associated virus-mediated gene transfer of mutant hPCSK9, Arterioscler. Thromb. Vasc. Biol. 35 (2015) 50–59, https://doi.org/10.1161/ATVBAHA.114.303617.

[34] S. Kumar, D.W. Kang, A. Rezvan, H. Jo, Accelerated atherosclerosis development in C57Bl6 mice by overexpressing AAV-mediated PCSK9 and partial carotid ligation, Lab. Invest. 97 (2017) 935–945, https://doi.org/10.1038/labinvest.2017.47.

[35] G.A. Foster, R.M. Gower, K.L. Stanhope, P.J. Havel, S.I. Simon, E.J. Armstrong, On-chip phenotypic analysis of inflammatory monocytes in atherogenesis and myocardial infarction, Proc. Natl. Acad. Sci. U.S.A. 110 (2013) 13944–13949, https://doi.org/10.1073/pnas.1300651110.

[36] D.B. Germano, S.B. Oliveira, A.L.L. Bachi, Y. Juliano, N.F. Novo, J. Bussador do Amaral, C.N. Franca, Monocyte chemokine receptors as therapeutic targets in cardiovascular diseases, Immunol. Lett. 256–257 (2023) 1–8, https://doi.org/10.1016/j.imlet.2023.03.002.

[37] P. Ghoshal, B. Singla, H. Lin, D.M. Feck, N. Cantu-Medellin, E.E. Kelley, S. Haigh, D. Fulton, G. Csanyi, Nox2-Mediated PI3K and cofilin activation confers alternate redox control of macrophage pinocytosis, Antioxidants Redox Signal. 26 (2017) 902–916, https://doi.org/10.1089/ars.2016.6639.

[38] M. Bohdanowicz, S. Grinstein, Role of phospholipids in endocytosis, phagocytosis, and macropinocytosis, Physiol. Rev. 93 (2013) 69–106, https://doi.org/10.1152/physrev.00002.2012.

[39] K. Hirano, W.S. Chen, A.L. Chueng, A.A. Dunne, T. Seredenina, A. Filippova, S. Ramachandran, A. Bridges, L. Chaudry, G. Pettman, et al., Discovery of GSK2795039, a novel small molecule NADPH oxidase 2 inhibitor, Antioxidants Redox Signal. 23 (2015) 358–374, https://doi.org/10.1089/ars.2014.6202.

[40] T.S. Kapellos, L. Bonaguro, I. Gemund, N. Reusch, A. Saglam, E.R. Hinkley, J. L. Schultze, Human monocyte subsets and phenotypes in major chronic inflammatory diseases, Front. Immunol. 10 (2019) 2035, https://doi.org/10.3389/fimmu.2019.02035.

[41] L. Ziegler-Heitbrock, P. Ancuta, S. Crowe, M. Dalod, V. Grau, D.N. Hart, P. J. Leenen, Y.J. Liu, G. MacPherson, G.J. Randolph, et al., Nomenclature of monocytes and dendritic cells in blood, Blood 116 (2010) e74–e80, https://doi.org/10.1182/blood-2010-02-258558.

[42] B. Passlick, D. Flieger, H.W. Ziegler-Heitbrock, Identification and characterization of a novel monocyte subpopulation in human peripheral blood, Blood 74 (1989) 2527–2534.

[43] A.M. Zawada, K.S. Rogacev, B. Rotter, P. Winter, R.R. Marell, D. Fliser, G.H. Heine, SuperSAGE evidence for CD14++CD16+ monocytes as a third monocyte subset, Blood 118 (2011) e50–e61, https://doi.org/10.1182/blood-2011-01-326827.

[44] A.V. Ruder, S.M.W. Wetzels, L. Temmerman, E.A.L. Biessen, P. Goossens, Monocyte heterogeneity in cardiovascular disease, Cardiovasc. Res. 119 (2023) 2033–2045, https://doi.org/10.1093/cvr/cvad069.

[45] L.M. Varela, A. Ortega, B. Bermudez, S. Lopez, Y.M. Pacheco, J. Villar, R. Abia, F. J. Muriana, A high-fat meal promotes lipid-load and apolipoprotein B-48 receptor transcriptional activity in circulating monocytes, Am. J. Clin. Nutr. 93 (2011) 918–925, https://doi.org/10.3945/ajcn.110.007765.

[46] H. Wu, R.M. Gower, H. Wang, X.Y. Perrard, R. Ma, D.C. Bullard, A.R. Burns, A. Paul, C.W. Smith, S.I. Simon, et al., Functional role of CD11c+ monocytes in atherogenesis associated with hypercholesterolemia, Circulation 119 (2009) 2708–2717, https://doi.org/10.1161/CIRCULATIONAHA.108.823740.

[47] J. Persson, E. Degerman, J. Nilsson, M.W. Lindholm, Perilipin and adipophilin expression in lipid loaded macrophages, Biochem. Biophys. Res. Commun. 363 (2007) 1020–1026, https://doi.org/10.1016/j.bbrc.2007.09.074.

[48] I. Buers, O. Hofnagel, A. Ruebel, N.J. Severs, H. Robenek, Lipid droplet associated proteins: an emerging role in atherogenesis, Histol. Histopathol. 26 (2011) 631–642, https://doi.org/10.14670/HH-26.631.

[49] K.J. Woollard, F. Geissmann, Monocytes in atherosclerosis: subsets and functions, Nat. Rev. Cardiol. 7 (2010) 77–86, https://doi.org/10.1038/nrcardio.2009.228.

[50] K.W. Kim, S. Ivanov, J.W. Williams, Monocyte recruitment, specification, and function in atherosclerosis, Cells 10 (2020), https://doi.org/10.3390/cells10010015.

[51] Y.V. Bobryshev, Monocyte recruitment and foam cell formation in atherosclerosis, Micron 37 (2006) 208–222, https://doi.org/10.1016/j.micron.2005.10.007.

[52] C. Guijas, C. Meana, A.M. Astudillo, M.A. Balboa, J. Balsinde, Foamy monocytes are enriched in cis-7-hexadecenoic fatty acid (16:1n-9), a possible biomarker for

early detection of cardiovascular disease, Cell Chem. Biol. 23 (2016) 689–699, https://doi.org/10.1016/j.chembiol.2016.04.012.
[53] S.J. Bernelot Moens, S.L. Verweij, J.G. Schnitzler, L.C.A. Stiekema, M. Bos, A. Langsted, C. Kuijk, S. Bekkering, C. Voermans, H.J. Verberne, et al., Remnant cholesterol elicits arterial wall inflammation and a multilevel cellular immune response in humans, Arterioscler. Thromb. Vasc. Biol. 37 (2017) 969–975, https://doi.org/10.1161/ATVBAHA.116.308834.
[54] H.A. Dresel, D.P. Via, M. Stohr, U. Elchner, A. Gnasso, A. Postiglione, N. Blin, J. Augustin, G. Schettler, Observations on leukocytes from patients with severe familial hypercholesterolemia, Arteriosclerosis 6 (1986) 259–264, https://doi.org/10.1161/01.atv.6.3.259.
[55] S.O. Rahaman, D.J. Lennon, M. Febbraio, E.A. Podrez, S.L. Hazen, R.L. Silverstein, A CD36-dependent signaling cascade is necessary for macrophage foam cell formation, Cell Metabol. 4 (2006) 211–221, https://doi.org/10.1016/j.cmet.2006.06.007.
[56] H.Y. Huh, S.F. Pearce, L.M. Yesner, J.L. Schindler, R.L. Silverstein, Regulated expression of CD36 during monocyte-to-macrophage differentiation: potential role of CD36 in foam cell formation, Blood 87 (1996) 2020–2028.
[57] M.S. Woo, J. Yang, C. Beltran, S. Cho, Cell surface CD36 protein in monocyte/macrophage contributes to phagocytosis during the resolution phase of ischemic stroke in mice, J. Biol. Chem. 291 (2016) 23654–23661, https://doi.org/10.1074/jbc.M116.750018.
[58] M. Moniuszko, K. Kowal, M. Rusak, M. Pietruczuk, M. Dabrowska, A. Bodzenta-Lukaszyk, Monocyte CD163 and CD36 expression in human whole blood and isolated mononuclear cell samples: influence of different anticoagulants, Clin. Vaccine Immunol. 13 (2006) 704–707, https://doi.org/10.1128/CVI.00417-05.
[59] V.S. Peche, T.A. Pietka, M. Jacome-Sosa, D. Samovski, H. Palacios, G. Chatterjee-Basu, A.C. Dudley, W. Beatty, G.A. Meyer, I.J. Goldberg, et al., Endothelial cell CD36 regulates membrane ceramide formation, exosome fatty acid transfer and circulating fatty acid levels, Nat. Commun. 14 (2023) 4029, https://doi.org/10.1038/s41467-023-39752-3.
[60] A. Ghosh, G. Murugesan, K. Chen, L. Zhang, Q. Wang, M. Febbraio, R.M. Anselmo, K. Marchant, J. Barnard, R.L. Silverstein, Platelet CD36 surface expression levels affect functional responses to oxidized LDL and are associated with inheritance of specific genetic polymorphisms, Blood 117 (2011) 6355–6366, https://doi.org/10.1182/blood-2011-02-338582.
[61] S. Mosig, K. Rennert, P. Buttner, S. Krause, D. Lutjohann, M. Soufi, R. Heller, H. Funke, Monocytes of patients with familial hypercholesterolemia show alterations in cholesterol metabolism, BMC Med. Genom. 1 (2008) 60, https://doi.org/10.1186/1755-8794-1-60.
[62] C. Commisso, S.M. Davidson, R.G. Soydaner-Azeloglu, S.J. Parker, J.J. Kamphorst, S. Hackett, E. Grabocka, M. Nofal, J.A. Drebin, C.B. Thompson, et al., Macropinocytosis of protein is an amino acid supply route in Ras-transformed cells, Nature 497 (2013) 633–637, https://doi.org/10.1038/nature12138.
[63] S. Takashiba, T.E. Van Dyke, S. Amar, Y. Murayama, A.W. Soskolne, L. Shapira, Differentiation of monocytes to macrophages primes cells for lipopolysaccharide stimulation via accumulation of cytoplasmic nuclear factor kappaB, Infect. Immun. 67 (1999) 5573–5578, https://doi.org/10.1128/IAI.67.11.5573-5578.1999.
[64] T. Starr, T.J. Bauler, P. Malik-Kale, O. Steele-Mortimer, The phorbol 12-myristate-13-acetate differentiation protocol is critical to the interaction of THP-1 macrophages with Salmonella Typhimurium, PLoS One 13 (2018) e0193601, https://doi.org/10.1371/journal.pone.0193601.
[65] J. Barlic, Y. Zhang, J.F. Foley, P.M. Murphy, Oxidized lipid-driven chemokine receptor switch, CCR2 to CX3CR1, mediates adhesion of human macrophages to coronary artery smooth muscle cells through a peroxisome proliferator-activated receptor gamma-dependent pathway, Circulation 114 (2006) 807–819, https://doi.org/10.1161/CIRCULATIONAHA.105.602359.
[66] J. Frostegard, J. Nilsson, A. Haegerstrand, A. Hamsten, H. Wigzell, M. Gidlund, Oxidized low density lipoprotein induces differentiation and adhesion of human monocytes and the monocytic cell line U937, Proc. Natl. Acad. Sci. U.S.A. 87 (1990) 904–908, https://doi.org/10.1073/pnas.87.3.904.
[67] J.M. Hayden, L. Brachova, K. Higgins, L. Obermiller, A. Sevanian, S. Khandrika, P. D. Reaven, Induction of monocyte differentiation and foam cell formation in vitro by 7-ketocholesterol, J. Lipid Res. 43 (2002) 26–35.
[68] Y. Shi, D. Kim, M. Caldwell, D. Sun, The role of Na(+)/h (+) exchanger isoform 1 in inflammatory responses: maintaining H(+) homeostasis of immune cells, Adv. Exp. Med. Biol. 961 (2013) 411–418, https://doi.org/10.1007/978-1-4614-4756-6_35.
[69] G.A. Foster, L. Xu, A.A. Chidambaram, S.R. Soderberg, E.J. Armstrong, H. Wu, S. I. Simon, CD11c/CD18 signals very late antigen-4 activation to initiate foamy monocyte recruitment during the onset of hypercholesterolemia, J. Immunol. 195 (2015) 5380–5392, https://doi.org/10.4049/jimmunol.1501077.
[70] K. Bedard, K.H. Krause, The NOX family of ROS-generating NADPH oxidases: physiology and pathophysiology, Physiol. Rev. 87 (2007) 245–313, https://doi.org/10.1152/physrev.00044.2005.
[71] A. Karlsson, C. Dahlgren, Assembly and activation of the neutrophil NADPH oxidase in granule membranes, Antioxidants Redox Signal. 4 (2002) 49–60, https://doi.org/10.1089/152308602753625852.
[72] A.W. Segal, The function of the NADPH oxidase of phagocytes and its relationship to other NOXs in plants, invertebrates, and mammals, Int. J. Biochem. Cell Biol. 40 (2008) 604–618, https://doi.org/10.1016/j.biocel.2007.10.003.
[73] M. Fujii, K. Kawai, Y. Egami, N. Araki, Dissecting the roles of Rac1 activation and deactivation in macropinocytosis using microscopic photo-manipulation, Sci. Rep. 3 (2013) 2385, https://doi.org/10.1038/srep02385.
[74] S. Yoshida, I. Gaeta, R. Pacitto, L. Krienke, O. Alge, B. Gregorka, J.A. Swanson, Differential signaling during macropinocytosis in response to M-CSF and PMA in macrophages, Front. Physiol. 6 (2015) 8, https://doi.org/10.3389/fphys.2015.00008.
[75] H. Younus, Therapeutic potentials of superoxide dismutase, Int. J. Health Sci. 12 (2018) 88–93.
[76] J.S. Jeeva, J. Sunitha, R. Ananthalakshmi, S. Rajkumari, M. Ramesh, R. Krishnan, Enzymatic antioxidants and its role in oral diseases, J. Pharm. BioAllied Sci. 7 (2015) S331–S333, https://doi.org/10.4103/0975-7406.163438.
[77] K. Piszczatowska, D. Przybylska, E. Sikora, G. Mosieniak, Inhibition of NADPH oxidases activity by diphenyleneiodonium chloride as a mechanism of senescence induction in human cancer cells, Antioxidants 9 (2020), https://doi.org/10.3390/antiox9121248.
[78] T.A. Jacinto, G.S. Meireles, A.T. Dias, R. Aires, M.L. Porto, A.L. Gava, E.C. Vasquez, T.M.C. Pereira, B.P. Campagnaro, S.S. Meyrelles, Increased ROS production and DNA damage in monocytes are biomarkers of aging and atherosclerosis, Biol. Res. 51 (2018) 33, https://doi.org/10.1186/s40659-018-0182-7.
[79] P.A. Barry-Lane, C. Patterson, M. van der Merwe, Z. Hu, S.M. Holland, E.T. Yeh, M. S. Runge, p47phox is required for atherosclerotic lesion progression in ApoE(-/-) mice, J. Clin. Invest. 108 (2001) 1513–1522, https://doi.org/10.1172/JCI11927.
[80] F. Xu, Y. Liu, L. Shi, W. Liu, L. Zhang, H. Cai, J. Qi, Y. Cui, W. Wang, Y. Hu, NADPH oxidase p47phox siRNA attenuates adventitial fibroblasts proliferation and migration in apoE(-/-) mouse, J. Transl. Med. 13 (2015) 38, https://doi.org/10.1186/s12967-015-0407-2.
[81] F.K. Swirski, P. Libby, E. Aikawa, P. Alcaide, F.W. Luscinskas, R. Weissleder, M. J. Pittet, Ly-6Chi monocytes dominate hypercholesterolemia-associated monocytosis and give rise to macrophages in atheromata, J. Clin. Invest. 117 (2007) 195–205, https://doi.org/10.1172/JCI29950.
[82] F. Tacke, D. Alvarez, T.J. Kaplan, C. Jakubzick, R. Spanbroek, J. Llodra, A. Garin, J. Liu, M. Mack, N. van Rooijen, et al., Monocyte subsets differentially employ CCR2, CCR5, and CX3CR1 to accumulate within atherosclerotic plaques, J. Clin. Invest. 117 (2007) 185–194, https://doi.org/10.1172/JCI28549.
[83] G. Thomas, R. Tacke, C.C. Hedrick, R.N. Hanna, Nonclassical patrolling monocyte function in the vasculature, Arterioscler. Thromb. Vasc. Biol. 35 (2015) 1306–1316, https://doi.org/10.1161/ATVBAHA.114.304650.
[84] S. Yona, K.W. Kim, Y. Wolf, A. Mildner, D. Varol, M. Breker, D. Strauss-Ayali, S. Viukov, M. Guilliams, A. Misharin, et al., Fate mapping reveals origins and dynamics of monocytes and tissue macrophages under homeostasis, Immunity 38 (2013) 79–91, https://doi.org/10.1016/j.immuni.2012.12.001.
[85] L.D. Tapp, E. Shantsila, B.J. Wrigley, B. Pamukcu, G.Y. Lip, The CD14++CD16+ monocyte subset and monocyte-platelet interactions in patients with ST-elevation myocardial infarction, J. Thromb. Haemostasis 10 (2012) 1231–1241, https://doi.org/10.1111/j.1538-7836.2011.04603.x.
[86] B.J. Wrigley, E. Shantsila, L.D. Tapp, G.Y. Lip, CD14++CD16+ monocytes in patients with acute ischaemic heart failure, Eur. J. Clin. Invest. 43 (2013) 121–130, https://doi.org/10.1111/eci.12023.
[87] K.S. Rogacev, B. Cremers, A.M. Zawada, S. Seiler, N. Binder, P. Ege, G. Grosse-Dunker, I. Heisel, F. Hornof, J. Jeken, et al., CD14++CD16+ monocytes independently predict cardiovascular events: a cohort study of 951 patients referred for elective coronary angiography, J. Am. Coll. Cardiol. 60 (2012) 1512–1520, https://doi.org/10.1016/j.jacc.2012.07.019.
[88] A. Schlitt, G.H. Heine, S. Blankenberg, C. Espinola-Klein, J.F. Dopheide, C. Bickel, K.J. Lackner, M. Iz, J. Meyer, H. Darius, et al., CD14+CD16+ monocytes in coronary artery disease and their relationship to serum TNF-alpha levels, Thromb. Haemostasis 92 (2004) 419–424, https://doi.org/10.1160/TH04-02-0095.
[89] K.S. Rogacev, S. Seiler, A.M. Zawada, B. Reichart, E. Herath, D. Roth, C. Ulrich, D. Fliser, G.H. Heine, CD14++CD16+ monocytes and cardiovascular outcome in patients with chronic kidney disease, Eur. Heart J. 32 (2011) 84–92, https://doi.org/10.1093/eurheartj/ehq371.
[90] K.S. Rogacev, A.M. Zawada, I. Emrich, S. Seiler, M. Bohm, D. Fliser, K.J. Woollard, G.H. Heine, Lower Apo A-I and lower HDL-C levels are associated with higher intermediate CD14++CD16+ monocyte counts that predict cardiovascular events in chronic kidney disease, Arterioscler. Thromb. Vasc. Biol. 34 (2014) 2120–2127, https://doi.org/10.1161/ATVBAHA.114.304172.
[91] K.L. Wong, J.J. Tai, W.C. Wong, H. Han, X. Sem, W.H. Yeap, P. Kourilsky, S. C. Wong, Gene expression profiling reveals the defining features of the classical, intermediate, and nonclassical human monocyte subsets, Blood 118 (2011) e16–e31, https://doi.org/10.1182/blood-2010-12-326355.
[92] H. Williams, C. Mack, R. Baraz, R. Marimuthu, S. Naralashetty, S. Li, H. Medbury, Monocyte differentiation and heterogeneity: inter-subset and interindividual differences, Int. J. Mol. Sci. 24 (2023), https://doi.org/10.3390/ijms24108757.
[93] A.C. Hearps, G.E. Martin, T.A. Angelovich, W.J. Cheng, A. Maisa, A.L. Landay, A. Jaworowski, S.M. Crowe, Aging is associated with chronic innate immune activation and dysregulation of monocyte phenotype and function, Aging Cell 11 (2012) 867–875, https://doi.org/10.1111/j.1474-9726.2012.00851.x.
[94] M.F. Keller, A.P. Reiner, Y. Okada, F.J. van Rooij, A.D. Johnson, M.H. Chen, A. V. Smith, A.P. Morris, T. Tanaka, L. Ferrucci, et al., Trans-ethnic meta-analysis of white blood cell phenotypes, Hum. Mol. Genet. 23 (2014) 6944–6960, https://doi.org/10.1093/hmg/ddu401.
[95] C. Poitou, E. Dalmas, M. Renovato, V. Benhamo, F. Hajduch, M. Abdennour, J. F. Kahn, N. Veyrie, S. Rizkalla, W.H. Fridman, et al., CD14dimCD16+ and CD14+ CD16+ monocytes in obesity and during weight loss: relationships with fat mass

and subclinical atherosclerosis, Arterioscler. Thromb. Vasc. Biol. 31 (2011) 2322–2330, https://doi.org/10.1161/ATVBAHA.111.230979.
[96] C.S. McAlpine, M.G. Kiss, S. Rattik, S. He, A. Vassalli, C. Valet, A. Anzai, C.T. Chan, J.E. Mindur, F. Kahles, et al., Sleep modulates haematopoiesis and protects against atherosclerosis, Nature 566 (2019) 383–387, https://doi.org/10.1038/s41586-019-0948-2.
[97] A.L. Slusher, T.M. Zuniga, E.O. Acevedo, Maximal exercise alters the inflammatory phenotype and response of mononuclear cells, Med. Sci. Sports Exerc. 50 (2018) 675–683, https://doi.org/10.1249/MSS.0000000000001480.